Description of exclusive processes in the Reggeized one-pion-exchange model

L. A. Ponomarev

Institute of Theoretical and Experimental Physics, Moscow

Fiz. Elem. Chastits At. Yadra. 7, 186–248 (January–March 1976)

The model of Reggeized one-pion exchange is applied to exclusive reactions with low multiplicity. A definite variant of the model (the OPER model) is applied to reactions in which one or two pions are produced in πN and NN collisions. Practically all the characteristics of these reactions are described quantitatively in a model with fixed parameters values: the energy dependence of the cross sections, the mass distributions for systems of two and three particles, the momentum-transfer distributions, the cms angular distributions of πN and $\pi\pi$ pairs, and the appearance of near-threshold peaks in the πN, $\pi\pi$, $\pi\pi\pi$, and $N\pi\pi$ systems (the Deck effect).

PACS numbers: 12.40.Mm, 12.40.Rr

INTRODUCTION

There is now available a large amount of diverse experimental information on particle-production processes at medium and high energies (up to about 1500 GeV) for exclusive experiments, i. e., experiments in which all the particles are identified and their four-momenta measured. In order to elucidate the mechanism of inelastic processes, it is important to attempt to describe quantitatively this complete set of data in the framework of some simple model.

We set forth here the results of applying the Reggeized one-pion-exchange model to the production of one or two pions in NN and πN collisions in the energy range 2–205 GeV.

Wherein lies the difficulty in the theoretical description of multiple particle-production processes? In the first place, in the large number of independent kinematic variables. For comparison, let us consider some two-particle process, for example, elastic πN scattering. We set ourselves the task of describing approximately (with error ± 20%) the differential cross section at sufficiently high energies. We write the amplitude as a sum of the contributions of the Regge poles P, P', and ρ:

$$T_{\pi N}=\sum_i \gamma_i \exp(R_i^2 t)\,\eta_i(t)\,(s/s_0)^{\alpha_i(t)}, \quad i=P,\ P',\ \rho; \tag{1}$$

where $\eta_i(t)$ is the signature factor; γ_i and R_i^2 are parameters characterizing the residues of the Regge poles. If the nucleon spin is taken into account, two helicity amplitudes must be associated with each of the poles; however, bearing in mind the nature of the experimental data, as a first approximation we shall ignore the contribution of the poles P and P' to the amplitude with change of helicity. Then, in order to describe the differential cross sections of the various channels of elastic πN scattering and charge exchange, at least eight free parameters are needed. The parameters of the trajectories are assumed known.

What occurs on the transition to particle-production processes? Apparently, the picture must become much more complicated. Let us consider, for example, the production of a π^+ meson in a $\pi^- p$ collision at a few GeV:

$$\pi^- p \to \pi^-\pi^+ n. \tag{2}$$

In view of the success of the theory of complex angular momenta in the description of two-particle reactions, one would naturally attempt to apply it to inelastic processes. This was done for the first time by Ter-Martirosyan.[1] Among the concrete multireggeon models, the most widely used is the Chan–Loskiewicz–Allison model.[2] In these models, the phase space of the reaction (2) must be split into several kinematic regions, of which the most important are those corresponding to the production of resonances in the $\pi^-\pi^+$ and $\pi^+ n$ systems and the region in which all the two-particle masses are large. With allowance for what we have said, we describe the reaction (2) by the graphs

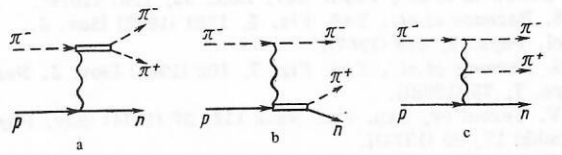

(3)

(the wavy lines correspond to the exchange of Regge poles).

Considering different resonances and Regge poles, one can attempt to describe the reaction cross section (2).

A pole with negative G parity (π, A_2) can contribute to graph a; with positive G parity (P, P', ρ), to graph b; and a pair of Regge poles with different G parities $[(P,\pi), (P',\pi), (P, A_2)]$, to graph c.

Since each reggeon pair or each reggeon–resonance pair has its own parameters, the total number of free parameters may be very large (many more than ten).

However, virtually all the experimental data on the reaction (2) can be described by means of one graph corresponding to the exchange of a Reggeized pion:

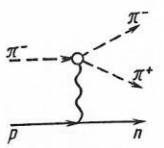

(4)

by introducing just one or two free parameters. The amplitude corresponding to this graph contains the block of elastic $\pi\pi$ scattering off the mass shell of one of the pions. The free parameter characterizes the form factor describing the departure of the amplitude from the mass shell. There is only one graph here, but it contains quite a lot: diagrams corresponding to the

production of resonances (ρ, f) in the $\pi^-\pi^+$ system by the exchange of the π pole (Fig. 3a) and two-reggeon diagrams corresponding to the exchange of (πP), $(\pi P')$, and $(\pi\rho)$ pole pairs (3c). It is important that all the constants in these graphs are fixed and determined by the on-shell $\pi^+\pi^-$ scattering amplitude.

Why is pion exchange singled out in the background of the other poles? It is frequently said that exchange of the π pole predominates only when $|t| \sim \mu^2$ (μ is the pion mass), and the contribution of the region with these small momentum transfers to the cross section of the various processes is small, so that pion exchange should not be singled out. In fact, the parameter is not μ^2 but some mass characteristic of the strong interaction, and it is approximately equal to 0.5–1 GeV.

Let us consider this more closely.

Let us consider the peripheral production of the two beams and compare the contribution of pion exchange with the exchange of any other particle, say, the ρ meson:

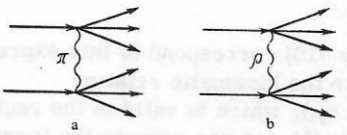

(5)

The contribution of diagram 5a to the cross section is proportional to $f_\pi/(t-\mu^2)^2$, and that of diagram 5b, to $f_\rho/(t-m_\rho^2)^2$, where f_π and f_ρ are unknown functions (there is no interference between the graphs). If it is assumed that these functions are approximately equal, then even at comparatively large momentum transfers—about 0.5 $(\text{GeV}/c)^2$—the contribution from the exchange of the pion is four times larger than that of the ρ meson. Analysis of the experimental data and model estimates show that f_π is actually greater than f_ρ in inelastic processes, and this enhances pion exchange even more. In the majority of elastic processes, pion exchange is either forbidden (πN or kN scattering), or strongly suppressed by the vanishing of the vertex for pion emission by a nucleon at zero momentum transfer (elastic NN and $N\bar{N}$ scattering).

On the other hand, it has long been known that quasielastic reactions like $pp \to \Delta^{++}n$, $\pi^-p \to \rho^0 n$, $\pi^+p \to \rho^0\Delta^{++}$, among others, can well be described by means of the one-pion-exchange model (OPE). The OPE model has also been found to describe experimental data well when it is applied to a number of processes of production of one or two pions in the full phase space (without singling out of resonances): $pp \to p\pi^+n$, $\pi^-p \to \pi^-\pi^+n$, $pp \to pp\pi^+\pi^-$, $\bar{p}p \to \bar{p}p\pi^+\pi^-$, $\pi^\pm p \to \pi^\pm\pi^+\pi^-p$, etc. It would be difficult to review all the investigations of this problem; we shall consider here only the papers of Wolf[3] (exchange of an elementary pion) and Berger[4] (exchange of a Reggeized pion), although the majority of experimental publications concerning processes of this type describe the data with some variant of the OPE model. There are indications that pion exchange is dominant in the production of three or more pions,[5] in inclusive processes,[6,7] and also in the production of heavy particles such as nucleon–antinucleon pairs.[8]

However, in the description of experimental data different modifications of one-pion models are used, and their parameters are changed for different processes and even for different energies within one particular process. There is no description of the experimental data in the framework of a single model with one system of parameters. The lack of correspondence between the models also appears in the Reggeization of the pion: Sometimes an elementary pion is exchanged, and sometimes a Reggeized pion. The existence of a pion trajectory with a slope of about 1 GeV^{-2} is the unequivocal conclusion of the analysis[9] of $\rho_{00}\, d\sigma/dt$ as a function of the energy in the reaction $\pi^-p \to \rho^0 n$.

In Refs. 10–17, a model of Reggeized one-pion exchange (OPER) was formulated with a view to describing processes with the production of pions in πN and NN collisions in a wide range of energies. In these papers, the OPER model was used for the quantitative description of the processes $pp \to pn\pi^+$ (Ref. 10), $np \to pp\pi^-$ (Ref. 11), and $\pi^-p \to \pi^-\pi^+n$ (Ref. 12). In Ref. 13, the model was used to analyze multiple production of pions in $\pi\pi$ collisions and also to analyze qualitatively the inclusive spectra of secondary particles in πN and NN collisions. Quantitative calculations of the inclusive spectra of the proton in pp collisions and a qualitative analysis of the inclusive spectra in $p \to \pi^-$ double charge exchange in various beams were carried in Refs. 14 and 15. In addition, in Ref. 14 the model was used to describe exclusive processes of two-pion production in NN and πN collisions; the individual distributions in these reactions and the energy dependence of the cross sections was calculated.

In this review, the production of one or two mesons will be described in detail by a variant of the OPER model that, as in Ref. 16, in which the reaction $\pi^-p \to \pi^-\pi^+\pi^-p$ was studied, differs from the earlier model by containing fewer parameters and giving a better description of the experimental data.

1. FORMULATION OF THE MODEL

We obtain here the general form of the matrix elements corresponding to the contribution of Reggeized pion exchange to production of one and two pions. For greater clarity, we formulate the model for the example of the two diagrams

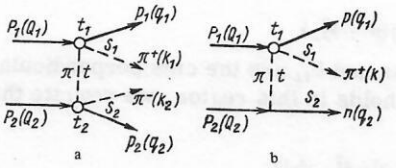

(6)

The two-block diagram (6a) determines the cross section of the reaction

$$pp \to pp\pi^+\pi^-, \tag{7a}$$

whereas the one-block diagram b determines the cross section of the reaction

$$pp \to pn\pi^+. \tag{7b}$$

As will be seen from what follows, processes with the production of two pions are better described by the

model and introduce more stringent restrictions on the general form of the form factor than processes with the production of one pion. In view of this, we shall consider first the expression for the matrix element corresponding to diagram (6a).

Amplitude of the two-block diagram. We denote by P_1 and P_2 the colliding protons and by p_1 and p_2 the created protons. We denote also by Q_1, Q_2, q_1, q_2 the momenta of the initial and the final protons and by k_1, k_2 the momenta of the created pions. In what follows, we shall need the notation

$$\left.\begin{aligned} &s=(Q_1+Q_2)^2;\quad s_1=(q_1+k_1)^2;\quad s_2=(q_2+k_2)^2;\quad s_3=(k_1+k_2)^2;\\ &t_1=(Q_1-q_1)^2;\quad t_2=(Q_2-q_2)^2;\quad t=(Q_1-q_1-k_1)^2=(Q_2-q_2-k_2)^2. \end{aligned}\right\}$$

We write the matrix element corresponding to the diagram (6a) in the form

$$M_a=F_2(t, s, s_1, s_2\ldots)\,T_{\pi^+p}(s_1, t_1, t)\,T_{\pi^-p}(s_2, t_2, t)/(t-\mu^2). \tag{8}$$

Here, $1/(t-\mu^2)$ is the pion propagator, which in the region of small $|t|$ is proportional to the signature factor $\eta_\pi(t)=\exp[-i\pi\alpha_\pi(t)/2]/\sin[\pi\alpha_\pi(t)/2]\approx 1/[\pi\alpha'_\pi(t-\mu^2)/2]$; $T_{\pi p}(S_i, t_i, t)$ are the off-shell elastic πp scattering amplitudes; F_2 is the form factor describing the factorized dependence of the departure from the mass shell of both amplitudes T_{π^+p} and T_{π^-p}.

What restrictions are there on the form of the function F_2? First, as $t\to\mu^2$ the expression (8) must correspond to the contribution of the pole diagram, i.e., $F_2\to 1$ as $t\to\mu^2$. Second, Reggeization of pion exchange requires that F_2 for $t\neq\mu^2$ have the form $F_2\sim(s_\pi/s_0)^{\alpha_\pi(t)}$ where s_π is the square of the invariant mass for the virtual pion; $\alpha_\pi(t)$ is the trajectory of the Regge π pole.

The concept of the invariant mass for pion exchange is vague but acquires a well defined meaning in the regions of the so-called three-reggeon kinematics. In these regions, all the two-particle masses are large but the momentum transfers are small. Depending on the longitudinal momenta of the particles, there are several such regions. The largest contribution to the cross section of the reaction (7a) comes from the configuration in which the longitudinal momenta of the protons in the common center-of-mass system are larger in magnitude than those of the pions (Fig. 1). In this region, $s_\pi=s_3$, so that the form factor must have the dependence $F_2\sim(s_3/s_0)^{\alpha_\pi(t)}$. Using the kinematic relation[17]

$$s_1s_2s_3=s\,(\mu^2+k_{1\perp}^2)\,(\mu^2+k_{2\perp}^2) \tag{9}$$

(μ is the pion mass and $k_{i\perp}$ are the cms perpendicular momenta), which holds in this region, we rewrite the form factor as

$$F_2=\left[\frac{s}{s_0}\,\frac{\mu^2+k_{1\perp}^2}{s_1}\,\frac{\mu^2+k_{2\perp}^2}{s_2}\right]^{\alpha_\pi(t)}. \tag{10}$$

In what follows, Eq. (10) will be the basis of the expression for the form factor in the complete phase space of the reaction (7a).[1)]

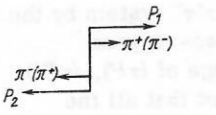

FIG. 1. Region in the space of longitudinal momentum that makes the greatest contribution to the cross section of the reaction (3).

Some of the most interesting regions of the reaction (7a) are the two-reggeon regions, in which one of the two-particle masses is small (a resonance mass), and all the others are large. All the momentum transfers are small, as before. The diagram corresponding to one of these kinematic regions has the form

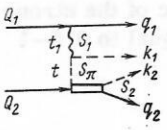

(11)

In it,

$$s_1, s_3\gg m^2;\quad s_2\approx m^2;\quad t_1, t\ll m^2\quad (m^2\approx 1\ \text{GeV}^2). \tag{12}$$

In this region, $s_\pi=(q_2+k_2+k_1)^2$, and

$$F_2\approx[(q_2+k_2+k_1)^2/s_0]^{\alpha_\pi(t)}. \tag{13}$$

Does the form factor (10) correspond to this expression? In fact, if we use the kinematic relation $S_1(q_2+k_2+k_1)^2=S(\mu^2+k_{1\perp}^2)$, which is valid in the region (12) and is analogous to (9), we can rewrite the form factor (10) in the form

$$F_2=[(q_2+k_2+k_1)^2/s_0]^{\alpha_\pi(t)}\,[(k_{2\perp}^2+\mu^2)/s_2]^{\alpha_\pi(t)}. \tag{14}$$

The first factor in (14) is equal to the expression (13), whereas the second can be interpreted as a particular form of the residue of the Regge pion pole for the process shown in the diagram (11). In particular, this factor leads to a definite dependence on the Treiman–Yang angle in the center-of-mass system of the created resonance.

Assuming that the pion trajectory is linear, $\alpha_\pi(t)=\alpha'_\pi(t-\mu^2)$, we rewrite the form factor in the more convenient exponential form

$$F_2=\exp\left\{\left[R_2^2+\alpha'_\pi\ln\left(\frac{s}{s_0}\,\frac{k_{1\perp}^2-\mu^2}{s_1}\,\frac{k_{2\perp}^2-\mu^2}{s_2}\right)\right](t-\mu^2)\right\}. \tag{15}$$

Here, $s_0=1$ GeV^2; R_2^2 is a free parameter.

Turning to the description of the experimental data, a natural first step would be to take the form factor in the form (12) and assume that it contains all the dependence of the πN scattering amplitudes on the departure from the mass shell, i.e., to set $T_{\pi^\pm p}(s_i, t_i, t)=T_{\pi^\pm p}(s_i, t_i, \mu^2)$ in Eq. (8). However, two facts were noted when this theory was compared with experiment.

First, it was found that in the off-shell πN scattering amplitude the vacuum pole is singled out, and this has a stronger dependence on the mass of the virtual pion (t) than does the resonance part of the amplitude or the other Regge poles (ρ and P'). To take this into account, we multiply the amplitude corresponding to the contribution of the vacuum pole to off-shell elastic πN scattering by a decreasing exponential function:

$$T_{\pi N}^p(s_i, t_i, t)=T_{\pi N}^p(s_i, t_i, \mu^2)\exp[R_p^2(t-\mu^2)]. \tag{16}$$

[1)] In regions in which the longitudinal momenta of the pions are larger in magnitude than those of the protons, S_π is certainty not equal to S_3, and the form factor must be different. However, calculations show that these regions make a small contribution to the total cross section (in particular, because of the large difference between the masses of the nucleon and the pion).

Second, it was found that the effective radius in (15) is smaller than the value observed experimentally at large momentum transfers $|t| \gtrsim 1$ GeV^2. The increase in the slope at large momentum transfers with retention of the factorization of the expression (15) could be due to a change in the factors containing the perpendicular momenta:

$$k_{i\perp}^2 - \mu^2 \to k_{i\perp}^2 - \mu^2 - c(t-\mu^2). \tag{17a}$$

It should be warned that this procedure is not unique, but it leads to a successful description of the experimental data and requires the addition of only one extra parameter (c), and we shall therefore use this procedure.

In Ref. 10, the off-shell p-wave πN scattering amplitude, $T_{\pi N}^{I=1}(s_i, t_i)$, was expressed by means of an additional factor obtained in perturbation calculations in the resonance model:

$$T_{\pi N}^{I=1}(s_i, t_i, t) = \frac{Q(s_i, t_i, t)}{Q(s_i, t_i, \mu^2)} \exp\left[R_\Delta^2 (t-\mu^2)\right] T_{\pi N}^{I=1}(s_i, t_i, \mu^2).$$

Here, Q is the modulus of the three-momentum of the pion in the center-of-mass system of the pion and the nucleon. Similar factors were obtained by Wolf[3] for the partial-wave amplitudes. The parameter R_Δ^2 was found in the region $|t| < 0.3$ GeV^2 and is equal to 2.75 GeV^{-2}. For this value of the parameter, the additional factor for $|t| < 0.3$ GeV^2 varies very weakly, reaching its maximal value (~ 1.1) at $t \approx -0.1$ GeV^2. Taking into account the strong correlation between R_Δ^2 and the other parameters, and wishing to simplify the model for the off-shell πN scattering amplitude, we shall ignore this factor. The analogous factor describing the additional dependence of the p-wave $\pi\pi$ scattering amplitude on the departure from the mass shell will have a stronger effect, and will be taken into account later.

Finally, the form factor corresponding to the diagram (6a) becomes

$$F_2 = \exp\left\{\left[R_2^2 + \alpha_\pi' \ln\left(\frac{s}{s_0}\frac{\varkappa_1^2}{S_1}\frac{\varkappa_2^2}{S_2}\right)\right](t-\mu^2)\right\}; \qquad \varkappa_i^2 = k_{i\perp}^2 + \mu^2 - c(t-\mu^2). \tag{17b}$$

The parameters of the model were fixed by the description of the experimental data for the reaction (7a) at different energies. With the slope $\alpha_\pi' = 0.7$ GeV^{-2} of the pion trajectory, the three free parameters of the model were found to be $R_2^2 = 0.8$ GeV^{-2}, $R_p^2 = 1.3$ GeV^{-2}, and $c = 0.08$ ($\alpha_\pi' = 0.7$ GeV^{-2}).

The slope of the pion trajectory is not a free parameter since it cannot be determined independently (analysis of the reaction $\pi^- p \to \pi^-\pi^+ n$ gives the slope $\alpha_\pi' \approx 1 \pm 0.3$ GeV^{-2}). A change in the slope must be compensated by a change in the parameter R_2^2. To demonstrate the scale of the variation, we give another set of parameters that lead to an almost equivalent description of the reaction (7a): $R_2^2 = 1.6$ GeV^{-2}, $R_p^2 = 1.3$ GeV^{-2}, $c = 0.08$ ($\alpha_\pi' = 1$ GeV^{-2}).

We emphasize that the values of the parameters R_2^2, c, and α_π' are strongly correlated. Since theory and experiment were compared "by eye", too great significance should not be given to the choice of a particular set of parameters. It is probably more important that one can describe almost all the experimental data on the reaction (7a) in the simple model with just three free parameters.

Squaring Eq. (8)[2)] and summing over the spins, we obtain the following value for the square of the modulus of the matrix element:

$$\overline{|M_a|^2} = \frac{F_2^2}{(t-\mu^2)^2}\left[(8\pi)^2 S_1 \frac{d\sigma_{\pi+p}(S_1, t_1, t)}{d\Omega_1}\right]\left[(8\pi)^2 S_2 \frac{d\sigma_{\pi-p}(S_2, t_2, t)}{d\Omega_2}\right]. \tag{18}$$

A dependence on the departure from the mass shell occurs in the differential cross sections $d\sigma_\pi(S_i, t_i, t)/d\Omega_i$ in Eq. (18) because of the additional dependence on the t contribution of the vacuum pole to the πN scattering amplitude in Eq. (16).

Amplitude of the one block diagram. We denote by P_1 and P_2 the colliding protons and by Q_1, Q_2, q_1, q_2 and k the momenta of the two colliding protons, the created proton, the neutron, and the π^+ meson, respectively. We also introduce

$$\left.\begin{aligned} &s = (Q_1+Q_2)^2; \quad s_1 = (q_1+k)^2; \quad s_2 = (q^2+k)^2; \\ &t_1 = (Q_1-q_1)^2; \quad t = (Q_2-q_2)^2. \end{aligned}\right\} \tag{19}$$

We write the amplitude corresponding to the diagram (6b) in the form

$$M_b = G\sqrt{2}\,\bar{u}(q_2)\gamma_5 u(Q_2) F_1(t, S, S_1, \ldots) T_{\pi+p}(s_1, t_1, t)/(t-\mu^2). \tag{20}$$

Here, $G\sqrt{2}\bar{u}(q_2)\gamma_5 u(Q_2)$ is the vertex of π^+-meson emission by the proton ($G^2/4\pi = 14.6$).

We shall seek to determine F_1, like F_2, from the condition of Reggeization of the pion exchange. In the region satisfying the condition of two-reggeon kinematics $S \gg S_1 \gg m^2$, $S \gg S_2 \gg m^2$, $t_1, t \lesssim m^2$, $m^2 \approx 1$ GeV^2, F_1 must have the form $(S_2/S_0)^{\alpha_\pi(t)}$. Using the relation $S_1 S_2 = S(\mu^2 + k_\perp^2)$, which holds in this region and is analogous to (9), we reduce the form factor to

$$F_1 = \exp\left\{(R_1^2 + \alpha_\pi' \ln\left[s(\mu^2 + k_\perp^2)(s_i s_1)\right])(t-\mu^2)\right\}. \tag{21}$$

Here $s_0 = 1$ GeV^2 and R_1^2 is a free parameter.

In Ref. 10, to describe the reaction (7b), the form factor F_1 in the form (21) with $R_1^2 = 2.75$ GeV^{-2} was used. It was also assumed that the entire dependence on the departure from the mass shell is contained in the form factor, i.e., in Eq. (20): $T_{\pi+p}(S_1, t_1, t) = T_{\pi+p}(S_1, t_1, \mu^2)$. In this very simple variant, the model gives a successful quantitative description of virtually all the experimental data on the reaction (7b) for momenta of the incident proton from 2 to 30 GeV/c.

On the other hand, as we have already noted, reactions with the production of two pions require the introduction of an additional dependence on t for the contribution to the πN scattering amplitude of the vacuum pole in the form (16) and a change in the behavior of the form factor in the region $|t| \geq 1$ GeV^2 of the form (17a). Retaining the factorization properties of the form factors, it would be natural to attempt to describe the reaction (7b) under these two conditions.

[2)] The interference of the different graphs is small (not exceeding a few percent). Here, we do not consider effects associated with interference.

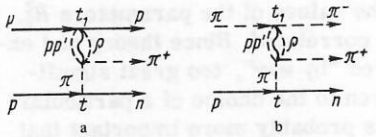

FIG. 2. Two-reggeon graphs for the reactions $pp \to pn\pi^+$ (a) and $\pi^- p \to \pi^-\pi^+ n$ (b).

In all the calculations that follow we shall use the form factor

$$F_1 = \exp\left\{\left(R_1^2 + \alpha_\pi' \ln\left[\frac{S\varkappa^2}{S_0 S_1}\right]\right)(t-\mu^2)\right\}; \quad \varkappa^2 = \mu^2 + k_\perp^2 - c(t-\mu^2); \quad R_1^2 = 1.9 \text{ GeV}^{-2} \tag{22}$$

with an amplitude $T_{\pi N}(S_1, t_1, t)$ satisfying the condition (16).

Squaring (20), averaging, and summing over the spins of the nucleons, we obtain the following value for the square of the modulus of the matrix element:

$$|\overline{M\delta}|^2 = 2G^2 |t| F_1^2 [(8\pi)^2 s_1 \, d\sigma_{\pi^+ p}(s_1, t_1, t)/d\Omega_1]/(t-\mu^2)^2. \tag{23}$$

Amplitudes containing blocks of virtual $\pi\pi$ scattering. Above, we have obtained the amplitudes for the production of one or two pions in NN collisions; these were determined by the off-shell πN elastic scattering amplitudes. We now generalize the model to analogous processes in pion beams. The matrix elements of the corresponding processes naturally depend on the off-shell $\pi\pi$ scattering amplitude.

We note first that in this variant of the model the basic parameters (R_1^2, R_2^2, R_p^2, c) which characterize the dependence on the departure from the mass shell $(t-\mu^2)$ should not change; for consider the two-reggeon regions of the processes $pp \to p\pi^+ n$ and $\pi^- p \to \pi^-\pi^+ n$ at sufficiently high energies. Figure 2 shows the two-reggeon graphs. It can be seen that the two graphs differ only by the vertices connecting the p, p', and ρ Regge poles with the nucleon (see Fig. 2a) and pion (see Fig. 2b) lines. In the theory of Regge poles, the residues at these vertices depend only on the momentum transfer t_1 and do not carry information about the momentum t transferred from the proton to the neutron.

To be specific, we give the explicit form of the amplitudes corresponding to the two diagrams

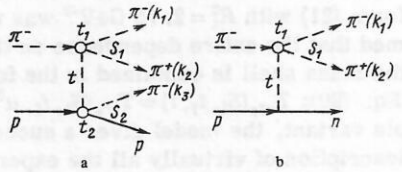

(24)

The diagram (24a) contributes to the cross section of the process $\pi^- p \to \pi^-\pi^-\pi^+ p$, and the diagram (24b) corresponds to the cross section of the process $\pi^- p \to \pi^-\pi^+ n$:

$$\left.\begin{aligned} &M_a = F_2 T_{\pi^-\pi^+}(S_1, t_1, t)\, T_{\pi^- p}(S_2, t_2, t)/(t-\mu^2); \\ &F_2 = \exp\{(R_2^2 + \alpha_\pi' \ln[s\varkappa_1^2\varkappa_2^2/S_0 S_1 S_2])(t-\mu^2)\}; \\ &\varkappa_1^2 = \begin{cases} \mu^2 + k_{2\perp}^2 - c(t-\mu^2), & \text{if } z_{\pi\pi} > 0; \\ \mu^2 + k_{1\perp}^2 - c(t-\mu^2), & \text{if } z_{\pi\pi} < 0. \end{cases} \\ &\varkappa_2^2 = \mu^2 + k_{3\perp}^2 - c(t-\mu^2). \end{aligned}\right\} \tag{25}$$

The diagram (24b) contributes to the cross section of the process $\pi^- p \to \pi^-\pi^+ n$:

$$\left.\begin{aligned} &M_\delta = G\sqrt{2}\, F_1 T_{\pi^-\pi^+}(S_1, t_1, t)\, \bar{u}_2 \gamma_5 u_1/(t-\mu^2); \\ &F_1 = \exp\{(R_1^2 + \alpha_\pi' \ln[S\varkappa^2/(S_0 S_1)])(t-\mu^2)\}; \\ &\varkappa^2 = \begin{cases} \mu^2 + k_{2\perp}^2 - c(t-\mu^2), & \text{if } z_{\pi\pi} > 0; \\ \mu^2 + k_{1\perp}^2 - c(t-\mu^2), & \text{if } z_{\pi\pi} < 0. \end{cases} \end{aligned}\right\} \tag{26}$$

In these expressions, $z_{\pi\pi}$ is the cosine of the scattering angle in the $\pi\pi$ scattering block in the center-of-mass system of the block. The selection conditions with respect to this angle, which appear in the definitions of $\varkappa_1^2$ and $\varkappa^2$, are needed to distinguish the configuration in which the π^- meson is faster than the π^+ meson from the opposite configuration in the common center-of-mass system. As we have already noted, the form factor must have a different dependence in these configurations. We recall that we ignored the corresponding change with proton transverse momentum in the dependence of the form factor on the transverse pion momentum in the πN scattering block [$\varkappa_2^2$ in (25)]. The form factor would have to be made more complicated to allow for this dependence, and it might be necessary to introduce new parameters.

The $\pi\pi$ scattering amplitudes $T_{\pi\pi}(S_1, t_1, t)$, like the πN scattering amplitudes, contain an additional dependence of the contribution of the vacuum pole on t in the form (16). In addition, in these amplitudes we have taken into account the additional dependence of the P-wave amplitude on the departure from the mass shell with a power cutoff in the form

$$T_{\pi\pi}^{I=1}(S_1, t_1, t) = \frac{Q(S_1, t_1, t)}{Q(S_1, t_1, \mu^2)} \frac{(1-c_\rho)}{(1-c_\rho Q(S_1, t_1, t)\, Q(S_1, t_1, \mu^2))} \times T_{\pi\pi}^{I=1}(S_1, t_1, \mu^2). \tag{27}$$

The value $c_\rho \approx 0.7$ was found for the parameter from analysis of the experimental data.

2. DESCRIPTION OF EXPERIMENTAL DATA

The model of Reggeized one-pion exchange was compared with the experimental data on production of one or two pions by means of the amplitudes obtained above with fixed values of the five free parameters: $R_1^2 = 1.9$ GeV^{-2}, $R_2^2 = 1.6$ GeV^{-2}, $R_p^2 = 1.3$ GeV^{-2}, $c = 0.08$, and $c_\rho = 0.7$, with the slope $\alpha_\pi' = 0.7$ GeV^{-2} of the pion trajectory. The calculations were performed on a computer using special mathematical programs intended for integration in the phase space of the created particles and adapted to the particular form of the matrix element. The Monte Carlo method was used for the integration and the errors in the calculations of the various distributions were a few percent. The on-shell elastic πN and $\pi\pi$ scattering amplitudes were tabulated. In the mass range $M_{\pi N} < 2$ GeV ($M_{\pi\pi} < 1.4$ GeV) phase-shift analysis was used; in the region of larger masses, Regge-pole parametrization (discussed in more detail in the Appendix) was used. Since each of the amplitudes decreases rapidly with increasing virtual mass of the

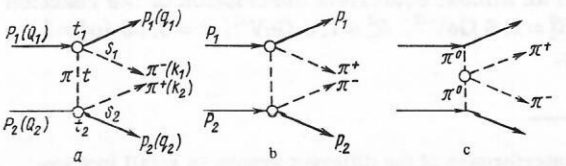

FIG. 3. Graphs corresponding to the reaction $pp \to pp\pi^+\pi^-$ in the OPER model.

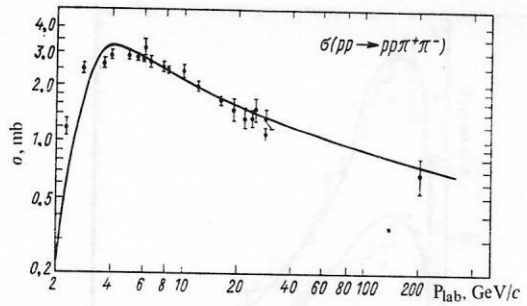

FIG. 4. Energy dependence of the cross section of the reaction (7a).

exchanged pion, the integration with respect to this variable was cut off at $|T_0| = 2$ GeV^2.

Description of the process $pp \to pp\pi^+\pi^-$

The reaction (7a) in the one-pion-exchange model corresponds to the three graphs shown in Fig. 3. In the calculations, only the squares of the amplitudes corresponding to Figs. 3a and 3b were used since the relative contribution of Fig. 3c, and also the contribution due to interference of different graphs, to the total cross section does not exceed a few percent.

We take the process (7a) as basic for determining the parameters R_2^2, R_p^2, and c, and we proceed from two facts: First, the matrix element determining this process depends only on the πN scattering amplitudes (see Fig. 3), which have been well studied experimentally, and not on the $\pi\pi$ scattering amplitudes, in whose values large uncertainties exist; second, the reaction (7a) has been well investigated experimentally in a wide range of energies up to 205 GeV.

The energy dependence of the cross section of the reaction (7a) is shown in Fig. 4. The theoretical curve corresponds well to the experimental data in the range

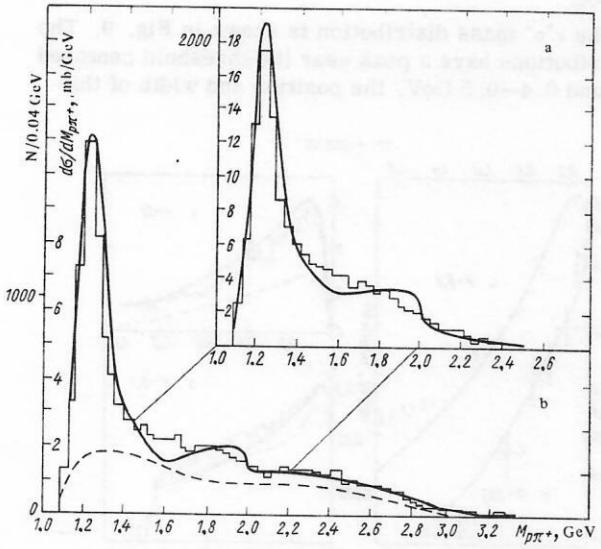

FIG. 5. Distributions with respect to the mass of the $p\pi^+$ system in the reaction (7a) at the momenta 6.6 GeV/c (a; Ref. 18) and 12 GeV/c (b; Ref. 19). The dashed curve is the contribution of combinations containing a pion and a nucleon from different blocks of Fig. 3.

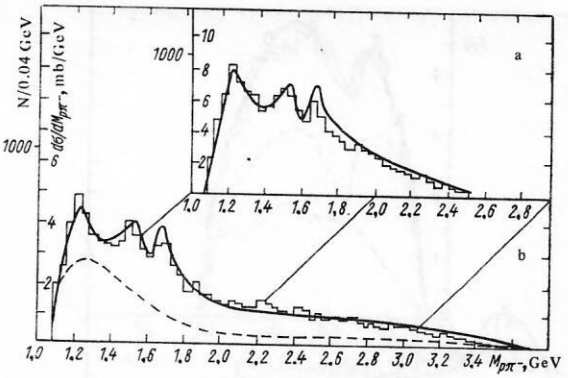

FIG. 6. Distributions with respect to the mass of the $p\pi^-$ system in the reaction (7a) at the momenta 6.6 GeV/c (a; Ref. 18) and 12 GeV/c (b; Ref. 19). The dashed curve is the contribution of combinations containing a pion and a nucleon from different blocks of Fig. 3.

of momenta from 3 to 205 GeV/c. With increasing energy, the rate of decrease of the cross section decreases. Theoretically, this is due to the presence of a vacuum pole in the πN scattering blocks. The rate of decrease of the cross section depends strongly on the parameter R_p^2. For example, at $R_p^2 = 0$ the total cross section of the reaction is almost independent of the energy.

The traditional variables whose distributions are studied experimentally at different energies are the following: the masses of the $p\pi^+$, $p\pi^-$, and $\pi^+\pi^-$ pairs; the mass of the three particles $p\pi^+\pi^-$; the square of the momentum t transferred from the initial proton p_i to the system $p_i\pi^+(p_i\pi^-)$; and the square of the momentum t_p transferred from the initial proton (p_i) to the final proton p_i ($i = 1, 2$). The distributions with respect to the masses of the $p\pi^+$, $p\pi^-$, and $p\pi^+\pi^-$ systems were obtained by symmetrizing with respect to the two final protons.

The distributions with respect to the masses of the

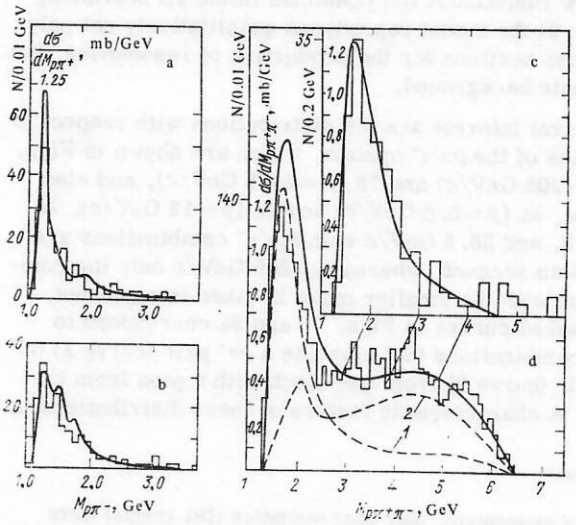

FIG. 7. Distributions with respect to the masses of the $p\pi^+$ (a) and $p\pi^-$ (b) systems at 205 GeV/c (Ref. 20) and with respect to the mass of the $p\pi^+\pi^-$ system at 205 and 28.5 GeV/c (c, d, respectively). Of the two $p_i\pi^+\pi^-$ combinations, only the one with the smaller mass was taken into account in plotting histogram c; 1) $p\pi^+$ combinations from one block; 2) $p\pi^-$ combinations from one block.

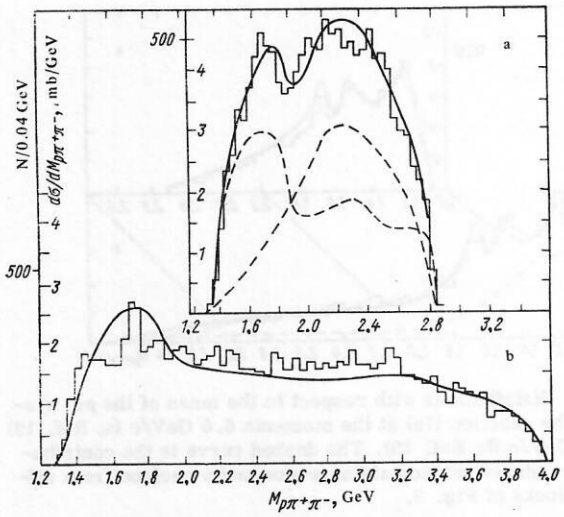

FIG. 8. Distributions with respect to the mass of the $p\pi^+\pi^-$ system at 6.6 and 12 GeV/c (a and b, respectively). The dashed curves are the same as in Fig. 7.

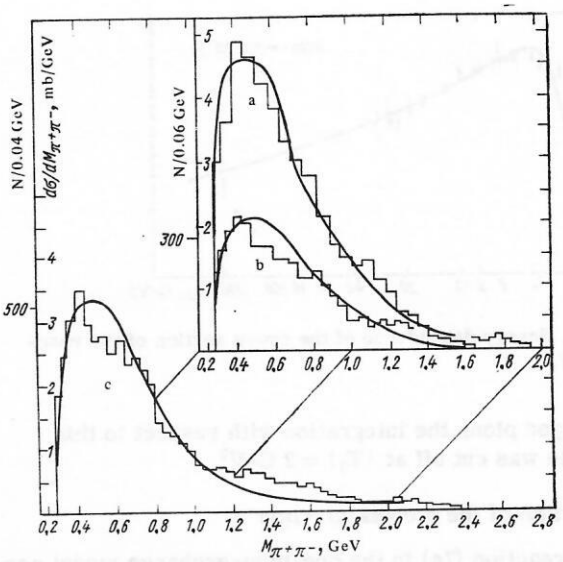

FIG. 9. Distributions with respect to the mass of the $\pi^+\pi^-$ system at 6.6, 24, and 12 GeV/c (a, b, c, respectively).

$p\pi^+$ and $p\pi^-$ systems at momenta 6.6 GeV/c (Ref. 18) and 12 GeV/c (Ref. 19) are given in Figs. 5 and 6, and those at 205 GeV/c are given in Figs. 7a and 7b (Ref. 20).[3] The dashed curves in Figs. 5b and 6b are the contribution of the combinations containing a pion and a nucleon from different blocks in the graphs of Figs. 3a and 3b. In what follows, we shall call these combinations "background combinations," in contrast to the main combinations for which the pion and nucleon belong to the same block. In the $p\pi^+$ system one observes a high peak in the region of the isobar $\Delta^{++}(1236)$, and in the $p\pi^-$ system three small peaks in the regions of the resonances $\Delta^0(1236)$, $N^*(1520)$, and $N^*(1960)$.[4] All these resonances are contained in the πN scattering blocks, and are therefore reproduced theoretically. In this connection, we note two circumstances: 1) Experimentally, one does not observe significant production of any new resonances not contained in the πN scattering blocks; 2) the model reproduces quantitatively not only the cross sections for the production of resonances, but also their background.

Of great interest are the distributions with respect to the mass of the $p\pi^+\pi^-$ system, which are shown in Figs. 7c ($p=205$ GeV/c) and 7d ($p=28.5$ GeV/c), and also in Figs. 8a ($p=6.6$ GeV/c) and 8b ($p=12$ GeV/c). At 6.6, 12, and 28.5 GeV/c both $p_i\pi^+\pi^-$ combinations are taken into account, whereas at 205 GeV/c only the combination with the smaller mass is taken into account. The dashed curves in Figs. 7b and 8a correspond to $p\pi^+\pi^-$ combinations that combine a $p\pi^+$ pair (curve 1) or $p\pi^-$ pair (curve 2) from one block with a pion from the other. A characteristic feature of these distributions is the peak with mass 1.7 GeV, its contribution to the total cross section increasing with increasing energy. The peak arises in the combination in which the $p\pi^+$ pair belongs to one block, which corresponds to the experimentally observed large width of the peak corresponding to decay into the isobar $\Delta^{++}(1236)$ and the π^- meson. (We recall that in the $M_{p\pi^+}$ mass distribution the isobar Δ^{++} is predominant.) From the fact that the absolute value of the cross section in the region of the peak hardly changes as the momentum is changed from 28.5 to 205 GeV/c we draw the following conclusion: At these energies, the peak is generated basically by exchange of the vacuum singularity. This peak in the model has a kinematic origin, and both the profile of the spectrum and the energy dependence of the spectrum are well reproduced theoretically. In the literature, the appearance of this peak is called the Deck effect.

The $\pi^+\pi^-$ mass distribution is shown in Fig. 9. The distributions have a peak near the threshold centered around 0.4–0.5 GeV, the position and width of this

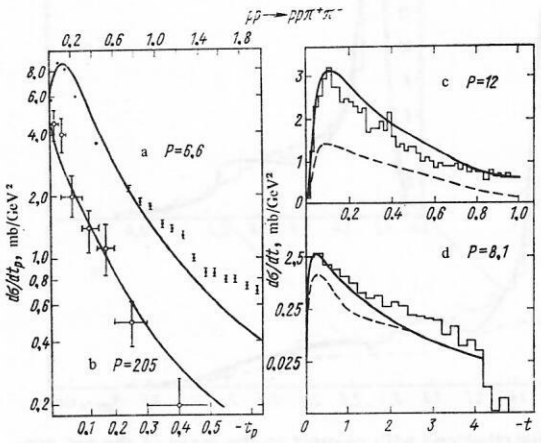

FIG. 10. Distributions with respect to the momentum transferred to the $p\pi^+\pi^-$ system at 6.6 and 205 GeV/c (a and b, respectively); ($M_{p\pi^+\pi^-}<3$ GeV) and the $p\pi^+$ ($p\pi^-$) system at 12 and 8.1 GeV/c (c and d, respectively).

[3] At this momentum, only poor statistics (191 events) were accumulated, so that the distributions could be plotted only with a large step.

[4] The jump in the distribution with respect to the mass $M_{p\pi^+}$ at the point $M_{p\pi}=2$ GeV is due to the poor fitting of the resonance amplitude and the Regge amplitude at this point (see the Appendix).

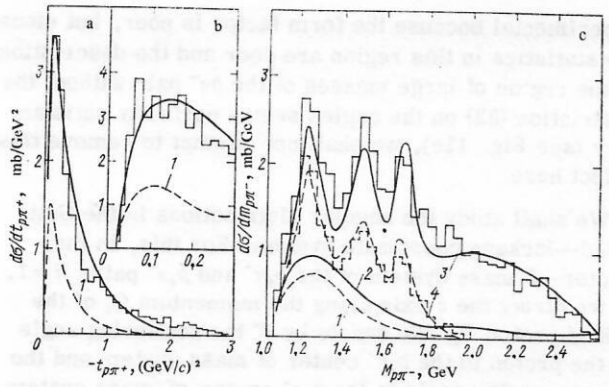

FIG. 11. Distributions with respect to the square of the momentum transferred to the isobar (a, b) and the mass $M_{p\pi^-}$ (c) in the reaction (29). 1) and 2) correspond to the background combinations; 2) and 3) correspond to the integral with respect to the total range of momentum transfers; 1(c) and 4 correspond to the additional restriction (31).

peak being practically independent of the energy. We emphasize that, in complete agreement with the model, Fig. 9 reveals virtually no trace of the ρ-meson peak which is usually observed in production of the $\pi^+\pi^-$ system in other reactions.[5)] On the one hand, the small cross section for production of the ρ meson indicates that there is a small contribution of the pole diagrams in which production of the ρ meson is allowed:

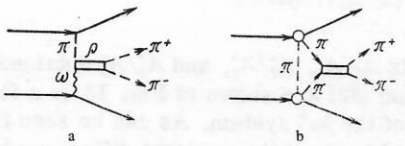

(28)

[for example, diagrams with the exchange of π^0 and ω^0 mesons (28a)]; on the other hand, it indicates that there is a small cross section of rescattering in the one-pion-exchange model (28b).

The distributions with respect to the momentum transferred from proton to proton, t_p, are shown in Figs. 10a and 10b. The upper scale corresponds to the data obtained at 6.6 GeV/c. The theoretical curve satisfactorily describes the experimental data right up to momentum transfers of about 1.5 GeV^2. The lower scale refers to the data obtained at 205 GeV/c. The experimental data are restricted to the region of low masses of the $p\pi^+\pi^-$ system ($M_{p\pi^+\pi^-} < 3$ GeV). Despite the wide variation of the energy and the nature of the distributions (the slope of the distributions varies by about a factor of 3), the theoretical curves describe the experimental data well.

The last distribution which remains to discuss is that with respect to the square of the momentum transferred from proton P_i to the $p_i\pi^+$ or $p_i\pi^-$ system [these two distributions are identical because of the symmetry of the reactions (7)]. This distribution is the one most directly related to the form factor F_2 and the one which is the most sensitive to a change of its parameters. Figures 10c and 10d are the experimental data obtained at 12 and 8.1 GeV/c. The dashed curves in these figures refer to the combinations consisting of a proton and a pion from different blocks, and can be regarded as backgrounds in the investigation of the form factor. It can be seen from the figures that the background makes a large contribution even in the region of very small momentum transfer, which considerably complicates the analysis of the form factor and makes it harder to extrapolate the experimental data to the pion pole.

Description of individual regions of the reaction $pp \to pp\pi^+\pi^-$. *Study of the reaction mechanism.* We have shown above that the model of Reggeized one-pion exchange gives a satisfactory quantitative description of the basic characteristics of the process (7a). The most pronounced structures in the mass distributions are the isobar $\Delta^{++}(1236)$ and the peak in the $p\pi^+\pi^-$ system around $M_{p\pi^+\pi^-} \approx 1.7$ GeV. Let us analyze these two structures in the model. As an additional verification of the model, we shall investigate the angular distributions in the center-of-mass systems of the $p\pi^+$ and $p\pi^-$ pairs when they are produced peripherally. It is well known[21] that these angular distributions are the ones most sensitive to the quantum numbers of the exchanged state.

The quasi-three-particle region of the reaction (7a)

$$pp \to p\pi^-\Delta^{++} \tag{29}$$

has been completely described in Ref. 18 for the momentum 6.6 GeV/c. In what follows, unless stated otherwise, the experimental data will be taken from Ref. 18. The distributions with respect to the square of the momentum transferred to the isobar are shown in Figs. 11a and 11b. To the mass of the isobar there corresponds the following interval of masses of the $p\pi^+$ system:

$$1.16 < M_{p\pi} < 1.3 \text{ GeV}. \tag{30}$$

The range of small momentum transfers is shown enlarged in the inset in Fig. 11b:

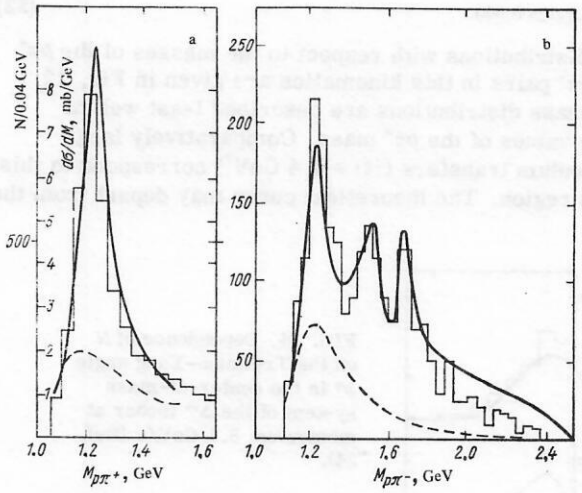

FIG. 12. Distributions with respect to $M_{p\pi^+}$ (a) and $M_{p\pi^-}$ (b) in the reaction (7) under the restrictions (32). The dashed curves are the background combinations.

[5)]The graphs of Figs. 3a and 3b do not contain resonances in the $\pi^+\pi^-$ system, whereas the graph 1c is proportional to the $\pi^+\pi^- \to \pi^0\pi^0$ cross section, in which there is no p-wave resonance of the ρ meson because the π^0 mesons are identical.

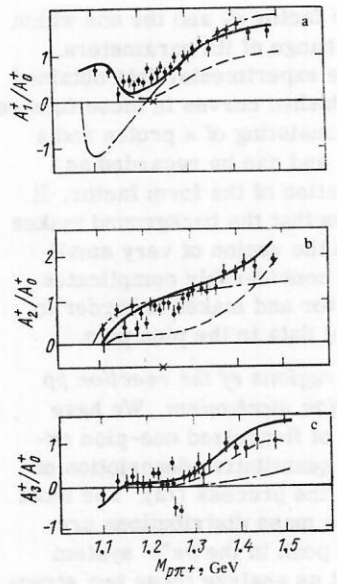

FIG. 13. Dependence of the coefficients A_e^+/A_0^+ on $M_{p\pi^+}$ under the restriction (32). The continuous curve is the theoretical calculation; the dashed curve, the contribution of the background combination; and the dot-dash-dot curve, the on-shell coefficient.

$$|t| < 0.3 \text{ GeV}^2. \tag{31}$$

The dashed curve is the contribution of the background combination, i.e., the combination of a proton and pion from different blocks. It can be seen from the figure that the relative contribution of the background combination is the same everywhere and equal to about 30%. The maximum of the background curve occurs at smaller momentum transfers than the maximum corresponding to the main combination. This makes it difficult to extrapolate the experimental data to the pion pole. Figure 11c is the distribution with respect to the mass of the $p\pi^-$ system subject to the restriction (30). Allowance for the background (see Fig. 11c) is most important in the region of the quasi-two-particle reaction $pp \to \Delta^{++}\Delta^0$.

In Ref. 18, a careful study was made of the angular distributions in the center-of-mass systems of the $p\pi^+$ and $p\pi^-$ pairs under the following restrictions on the cosine $z^*_{p\pi}$ of the angle between the emitted $p\pi$ pair in the common center-of-mass system:

$$|z^*_{p\pi}| > 0.965. \tag{32}$$

The distributions with respect to the masses of the $p\pi^+$ and $p\pi^-$ pairs in this kinematics are given in Fig. 12. The mass distributions are described least well at large values of the $p\pi^-$ mass. Comparatively large momentum transfers ($|t| \geq 0.4$ GeV^2) correspond to this mass region. The theoretical curve may depart from the experimental because the form factor is poor, but since the statistics in this region are poor and the description in the region of large masses of the $p\pi^-$ pair without the restriction (32) on the angles seems perfectly satisfactory (see Fig. 11c), we shall not attempt to remove this defect here.

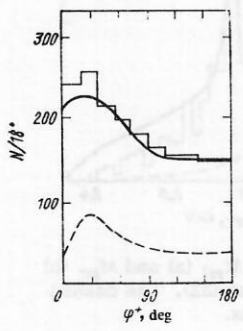

FIG. 14. Dependence of N on the Treiman–Yang angle φ^+ in the center-of-mass system of the Δ^{++} isobar at momentum 8.1 GeV/c (Ref. 24).

We shall study the angular distributions in the Gottfried–Jackson coordinate system. For this, in the center-of-mass system of the $p_i\pi^+$ and $p_i\pi^-$ pairs ($i = 1, 2$) we direct the z axis along the momentum Q_i of the initial proton P_i. We denote by θ^+ the scattering angle of the proton in the $p_i\pi^+$ center of mass system and the corresponding angle in the $p_i\pi^-$ center-of-mass system by θ^-. Following the four-momentum notation in Fig. 3, we also introduce azimuthal angles in these systems:

$$\varphi^{\pm} = \cos^{-1}\left(\frac{(\mathbf{Q}_i \times \mathbf{q}_i)(\mathbf{Q}_i \times \mathbf{Q}_j)}{|\mathbf{Q}_i \times \mathbf{q}_i||\mathbf{Q}_i \times \mathbf{Q}_j|}\right), \quad i, j = 1, 2;\ i \neq j. \tag{33}$$

Consider the angular distributions in the center-of-mass system of the $p\pi^+$ pair. Following Ref. 18, we shall characterize the distributions with respect to θ^+ by means of averaged Legendre polynomials:

$$A_l^+ A_0^+ = (2l+1)\langle P_l(\cos\theta^-)\rangle. \tag{34}$$

The on-shell differential cross section of π^+p scattering can be written by means of these coefficients in the form

$$\frac{d\sigma_{\pi^+p}}{d\Omega} = \frac{\sigma_{\pi^+p}}{4\pi}\sum_l (A_l^+/A_0^+) P_l(\cos\theta^-). \tag{35}$$

The coefficients A_1^+/A_0^+, A_2^+/A_0^+, and A_3^+/A_0^+ obtained under the condition (32) are shown in Fig. 13 as a function of the mass of the $p\pi^+$ system. As can be seen from Fig. 12a, one would expect the greatest difference between the angular distributions and the observed on-shell distributions in the region of small and large masses of the $p\pi^+$ pair, where the relative contribution of the background combination is maximal. This effect is observed in Figs. 13a–13c. Especially pronounced distortions arise in the A_0^+/A_1^+ curve at small masses. Thus, the model of one-pion exchange is well confirmed in the reaction (29) by the distribution with respect to the polar angle θ^+.

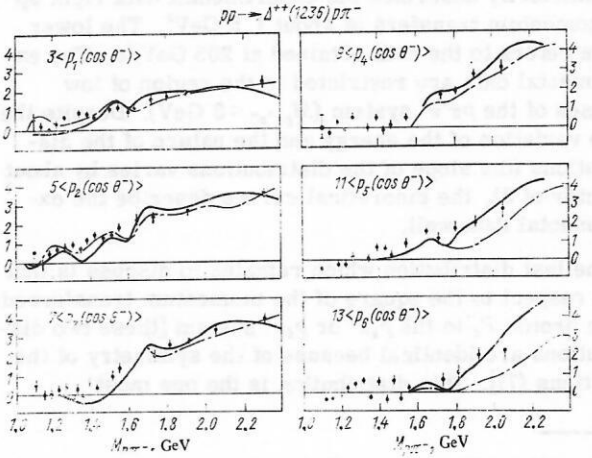

FIG. 15. Dependence of the coefficients A_i^-/A_0^- on the mass $M_{p\pi^-}$ under the restriction (32). The dot-dash-dot curves are the on-shell coefficients.

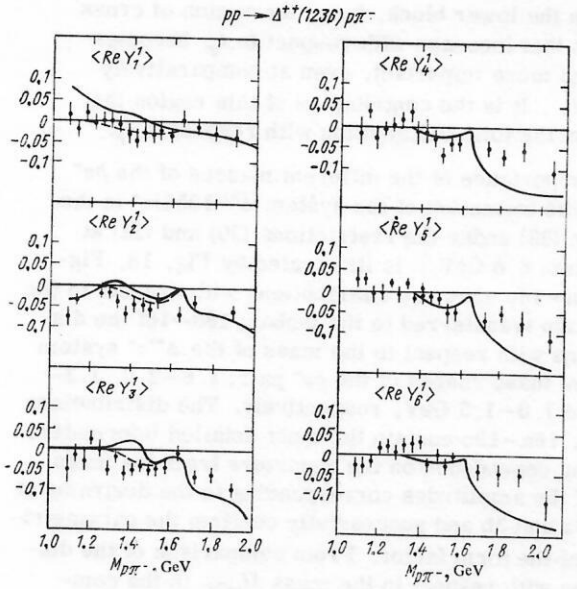

FIG. 16. Dependence of $\langle \mathrm{Re}\, Y_i^1 \rangle$ ($i = 1, 6$) on $M_{p\pi^-}$ under the restrictions (30) and (32). The dashed curves are the contribution of the background combination.

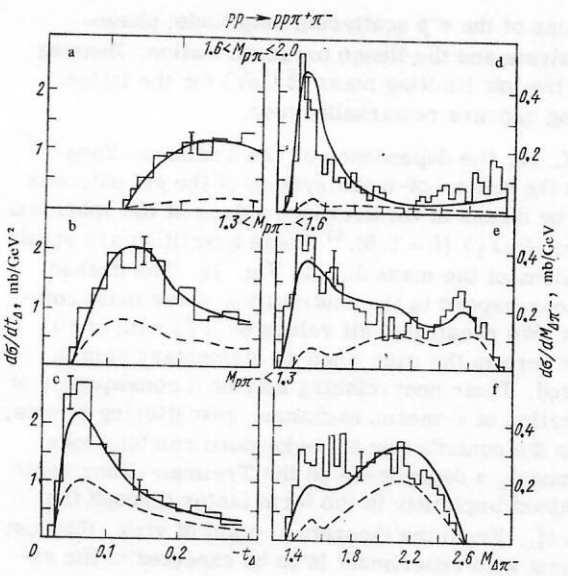

FIG. 18. Cross section as a function of the square of the momentum transferred to the isobar (a, b, c) and of the mass $M\Delta^{++}\pi$(d, e, f) under different restrictions on the mass $M_{p\pi^-}$. The dashed curves are the contribution of the background combination.

How critical is this distribution to the choice of the model? As a possible mechanism of the reaction (29) one could consider the exchange of other known Regge poles with isospin equal to unity: ρ or A_2. Since both trajectories, in contrast to the π-meson trajectory, have the natural spin-parity relation, it is be expected that the angular distributions for the decay of the isobar will differ in both cases from the distributions obtained here. To obtain an estimate, let us consider the coefficients A_1^+/A_0^+ and A_2^+/A_0^+ in the region of the isobar $\Delta^{++}(1236)$ in any reaction in which pion exchange is forbidden by G parity; for example, in the reaction $\pi^+ p \to \pi^0 \Delta^{++}$, to which only the ρ-meson pole contributes. As was noted in Ref. 22, the mean values of the elements of the density matrix of the Δ^{++} isobar in this reaction can be well described by the Stodolsky–Sakurai model,[23] according to which $\rho_{33} = \frac{3}{8}$, $\mathrm{Re}\rho_{3-1} = \sqrt{3}/8$, $\mathrm{Re}\rho_{31} = 0$. Calculating A^+/A_0^+ by means of the relation $A_2^+/A_0^+ = 2(0.5 - 2\rho_{33})$ and remembering that A_1^+/A_0^+ for a vector state is zero, we obtain these values for the coefficients:

$$A_1^+/A_0^+ = 0; \quad A_2^+/A_0^+ = -0.5. \tag{36}$$

Assuming factorization in the case of the exchange of trajectories with natural spin-parity relation, we can expect these coefficients (36) to have approximately the same values in the reaction (29) as well. These values are indicated in Figs. 13a and 13b by crosses. The coefficient A_1^+/A_0^+ is practically equal to its value obtained in this paper, while the coefficient A_2^+/A_0^+ differs appreciably. Taking into account its value (36) and also the deviation of the theoretical value at the mass $M_{p\pi} \approx 1.236$ GeV (~ 1) from the experimental value (~ 0.8), we can estimate the relative contribution of the ρ-meson trajectory:

$$W_\rho / W_\pi \approx 0.14. \tag{37}$$

The distribution with respect to the azimuthal angle φ^+ in the region of the isobar has been observed[24] at the momentum 8.1 GeV/c, and is shown in Fig. 14. As follows from the theoretical curves, both combinations, the main and the background (dashed curve) contribute to the observed asymmetry. We recall that there is an isotropic distribution in the case of the exchange of an elementary pion (state 0^-).

An even narrower region of phase space was investigated in the study of the angular distribution in the $p\pi^-$ system under the same condition (32). Whereas the angular distributions in the $p\pi^+$ system were investigated by integrating with respect to the mass of the $p\pi^-$ pair, the decay of the $p\pi^-$ system was studied with the mass of the $p\pi^+$ pair fixed by the condition (30).

The coefficients A_i^-/A_0^- are shown as functions of the mass $M_{p\pi^-}$ in Fig. 15. A systematic deviation of the theoretical curves and the experimental points from the dot-dash-dot curves is observed in the region of large masses and large angular momenta ($i \geq 4$). This deviation corresponds to an additional peaking of the angular distributions due to the indirect dependence of the form factor on the angles $\theta^\pm$ through the perpendicular components $k_\perp^2$ of the $\pi^\pm$-meson momenta. The behavior of the theoretical curves at the point $M_{p\pi^-} = 2$ GeV is an indication of the quality of the fitting of the two param-

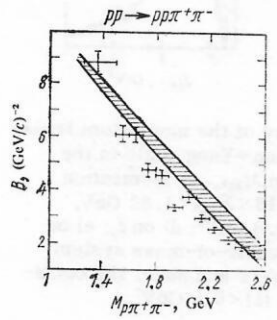

FIG. 17. Slope $B(M_{p\pi^+\pi^-})$ of the production cone of the $p\pi^+\pi^-$ system as a function of the mass of this system. The hatched region corresponds to the theoretical predictions for this quantity.

etrizations of the $\pi^- p$ scattering amplitude: phase-shift analysis and the Regge parametrization. Bearing in mind the low limiting mass (2 GeV) for the latter, the fitting appears remarkably good.

In Ref. 18, the dependence on the Treiman–Yang angle in the center-of-mass system of the $p\pi^-$ pair was studied by means of the averaged values of the spherical functions $\langle \mathrm{Re} Y_L^1 \rangle$ $(L = 1.6)$.[6] These quantities are shown as functions of the mass $M_{p\pi^-}$ in Fig. 16. The dashed curves correspond to the contribution of the main combination. We recall that all values of $\langle Y_L^M \rangle$ with $M \neq 0$ must be zero in the case when an elementary pion is exchanged. Their nonvanishing may be a consequence of Reggeization of π-meson exchange, rescattering effects, and also the contribution of background combinations. In the model, a dependence on the Treiman–Yang angle is contained implicitly in the form factor through the factors $k_{i\perp}^2$. From the theoretical point of view, the best agreement with experiment is to be expected in the region of the largest masses $M_{p\pi^-}$, since it was in this region that the model was formulated. From Fig. 16 it can be seen that the OPER model without allowance for rescattering effects gives a qualitative description of the behavior of $\langle \mathrm{Re} Y_L^1 \rangle$ in the resonance region of the mass of the $p\pi^-$ system as well.

The greatest discrepancy between the theoretical curves and the experimental points, both in Fig. 15 and Fig. 16, is observed in the region of masses $M_{p\pi^-} \approx 1.25$–1.45 GeV. It can also be seen from the figures that the discrepancy is due most likely to the background combination.

We now turn to a more detailed study of the conditions of creation and decay of the $p\pi^+\pi^-$ state in the reaction (7). The investigation of the cross section for the production of different mass ranges of the $p\pi^+\pi^-$ system as a function of the momentum transfer t_p revealed an interesting effect: If the dependence is parametrized in the form $\exp[B(M_{p\pi^+\pi^-})t_p]$, the coefficient B decreases strongly with increasing mass. The dependence $B(M_{p\pi^+\pi^-})$ measured at 6.6 GeV/c in Ref. 18 is shown in Fig. 17. The indeterminacy is due to the theoretically calculated cross section's not corresponding to a simple exponential.

The decrease in the slope can be understood roughly as follows. Consider, for example, the production of the $p\pi^+\pi^-$ system in the forward hemisphere (in the direction of the incident beam). If the minimal $M_{p\pi^+\pi^-}$ mass is created, the mass corresponding to the lower blocks in Figs. 3a and 3b is maximally large. The slope B, which determines the dependence on the momentum transferred from the proton P_2 to the proton p_2, is determined by the slope of the elastic $\pi^- p$ and $\pi^+ p$ scattering cross sections, which depend weakly on the mass of the πp system and are approximately 8–10 GeV^{-2}. With increasing mass $M_{p\pi^+\pi^-}$, the role of the small (resonance) masses of the lower blocks increases. At the same time, the region corresponding to backward scattering in the lower block, i.e., the region of cross sections that increase with respect to t_p, becomes more and more important, even at comparatively small $|t_p|$. It is the contribution of this region that broadens the total distribution with respect to t_p.

The importance of the different masses of the $p\pi^-$ pair in the formation of the system $\Delta^{++}(1236)\pi^-$ in the reaction (29) under the restrictions (30) and (31) at momentum 6.6 GeV/c is illustrated by Fig. 18. Figures 18a–18c show the distributions with respect to the momentum transferred to the isobar; 18d–18f the distributions with respect to the mass of the $\Delta^{++}\pi^-$ system for three mass ranges of the $p\pi^-$ pair: 1.6–2.0, 1.3–1.6, and 1.0–1.3 GeV, respectively. The distributions in Figs. 18a–18c contain the most detailed information about the dependence on the departure from the mass shell of the amplitudes corresponding to the diagrams of Figs. 3a and 3b and successfully confirm the parametrization of the form factor. From comparison of the distribution with respect to the mass $M_{p\pi^+\pi^-}$ in the complete phase space of the reaction (7) (see Fig. 8) with the distributions in Figs. 18d and 18f, one can see the displacement of the peak from around 1.7 GeV to the region 1.4–1.5 GeV. This effect is well reproduced by the model.

One of the most frequently investigated regions, for which simple models can be constructed, is the two-reggeon region of the reaction (29), which is determined by the condition that the momenta transferred to the isobar and the proton be sufficiently small and the mass of the $p\pi^-$ system be sufficiently large (above the resonances). It was in this region that the model of Reggeized one-pion exchange was first constructed.[4] The data of Figs. 18a and 18d apply to this region, in particular. Analogous regions have been investigated at 12 GeV/c (Figs. 19a–19c) (Ref. 19): $M_{p\pi^-}^2 > 3$ GeV^2, $|t_p| < 1$ GeV^2, $|t| < 0.8$ GeV^2, $1.15 < M_{p\pi^+} < 1.32$, and at

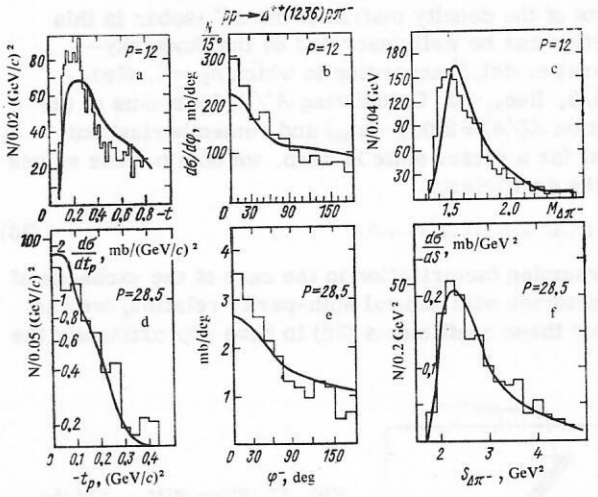

FIG. 19. Dependence: a) on the square of the momentum transferred to the isobar, b) on the Treiman–Yang angle in the $p\pi^-$ center-of-mass system, and c) on $M_{p\pi^+\pi^-}$ at momentum 12 GeV/c and under the conditions $1.16 < M_{p\pi^+} < 1.32$ GeV, $(M_{p\pi^-})^2 > 3$ GeV^2, $|t_p| < 1$ GeV^2, $|t| < 0.8$ GeV^2; d) on t_p; e) on the Treiman–Yang angle in the $p\pi^-$ center-of-mass system; and f) on $M_{\Delta^+\pi^-}^2$ at momentum 28.5 GeV/c and under the conditions $1.15 < M_{\pi^+} < 1.35$, $M_{p\pi^-} > 2$ GeV, $|t| < 0.8$ GeV^2.

[6]The mean values $\langle \mathrm{Re} Y_L^0 \rangle$ are proportional to A_L^-/A_0^-; the mean values $\langle \mathrm{Re} Y_L^M \rangle$ $(M > 1)$ were found experimentally to be nearly zero.

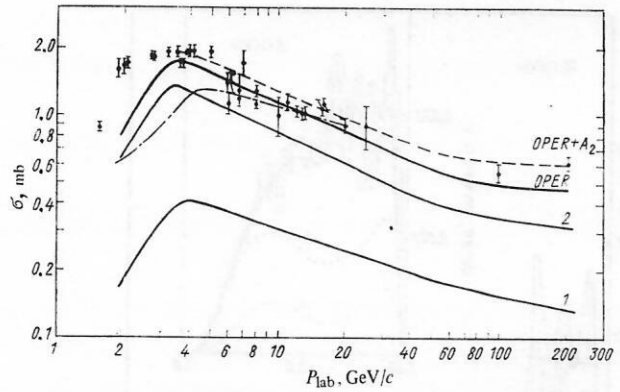

FIG. 20. Energy dependence of the cross section of the reaction (38). The dashed curve is the sum of the cross section calculated in the OPER model and the cross section for the production of the A_2 meson (0.14 mb) (Ref. 16); the dot-dash-dot curve is the curve calculated in Wolf's model[3]; 1) and 2) are the contributions of the individual diagrams.

28.5 GeV/c (see Figs. 19d–19f) (Ref. 4): $1.15 < M_{p\pi^+} < 1.35$, $M_{p\pi^-} > 2$ GeV, $|t| < 0.8$ GeV^2.

All the curves in Fig. 19 are normalized to the experimental data. The contribution of the background combinations is nowhere separated out, but it does not exceed 10% anywhere and does not affect the qualitative behavior of the curves. The theoretical description appears completely satisfactorily, although asymmetry with respect to the azimuthal angle in the experiment has been noted above.

Description of the Process $\pi^- p \to \pi^-\pi^+\pi^- p$[7)]

General characteristics. The reaction

$$\pi^- p \to \pi^-\pi^+\pi^- p \qquad (38)$$

is one of the most studied reactions. It is one of the first hadron processes to which quantitative models, mainly the one-pion-exchange model, were applied. The reaction (38) has been described in most detail in Ref. 3 by Wolf, who showed that the OPE model reproduces well many distributions, including that with respect to the masses of the created particle pairs. The main shortcoming of Ref. 3 is that there is no Reggeization of the pion exchange, and the energy dependence of the reaction (38) at low energies is not well described.

An OPER model capable of describing the total cross section of the reaction (38) at momentum 4.5 GeV/c was proposed in Ref. 25. It enables one to describe the general characteristics of the reaction, but, in the form in which it is formulated in Ref. 25, it clearly cannot be extended to the two-reggeon regions of the reaction (38), which are important at high energies. A variant of the OPER model especially intended for description of these regions had been proposed earlier in Ref. 4

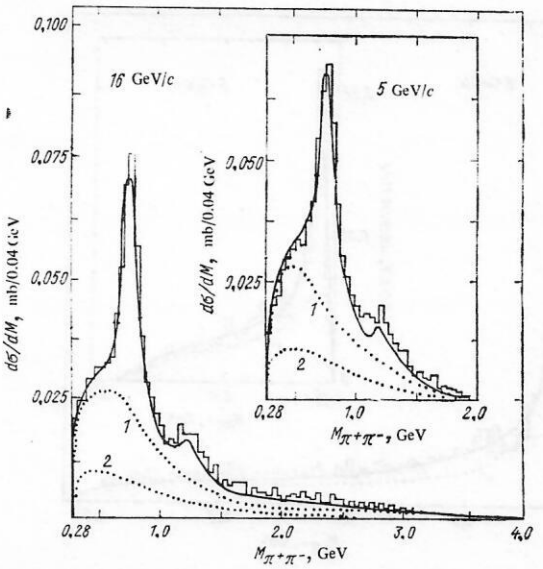

FIG. 21. Distributions with respect to the mass of the $\pi^+\pi^-$ pair in the reaction (38). 1) The contribution of the background combinations; 2) the contribution of the diagram (39a).

and, in a sense, it complements the variant considered in Ref. 25.

In what follows, we shall completely follow Ref. 16 in describing the reaction (38) in the OPER model. The main advantage of our approach is the almost complete absence of free parameters. The only free parameter, which appears on the transition from the reaction (7) to the reaction (38), is c_ρ, which is found from the condition of best agreement between the theoretical and the experimental data, and its value has been given immediately after Eq. (27).

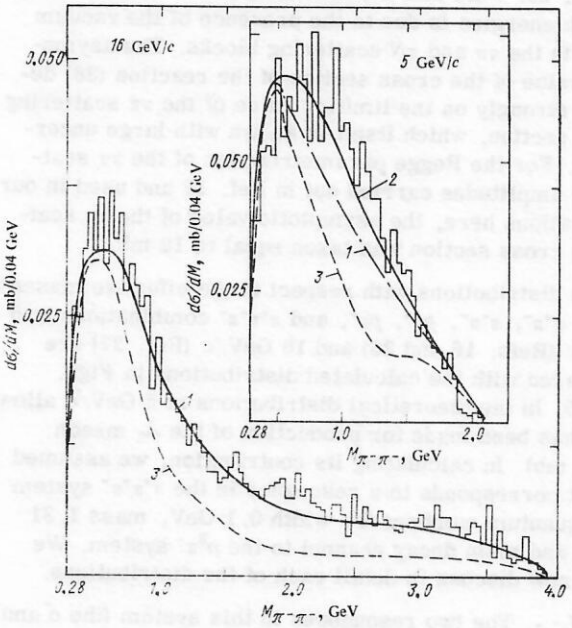

FIG. 22. Distributions with respect to the mass of the $\pi^-\pi^-$ pair in the reaction (38). 1) Calculation in the OPER model; 2) with allowance for the contribution of the A_2 meson; 3) contribution of the diagram (39b).

[7)] Calculations made by R. M. Lebedev have been used in this section. I am very grateful to him for making them available.

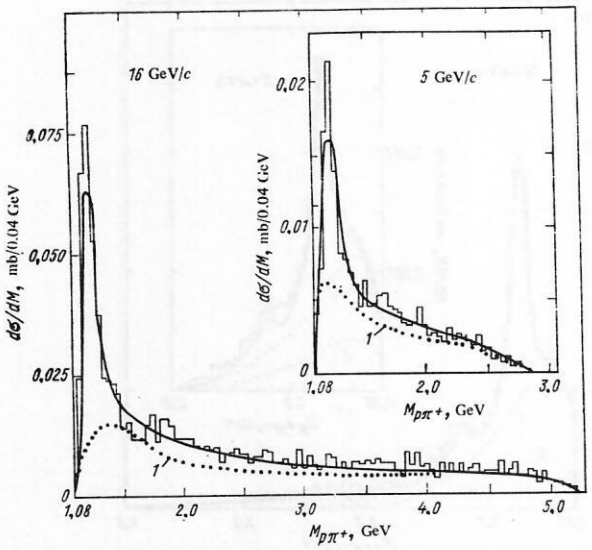

FIG. 23. Distribution with respect to the mass of the $p\pi^+$ pair in the reaction (38). 1) Contribution of the diagram (39b).

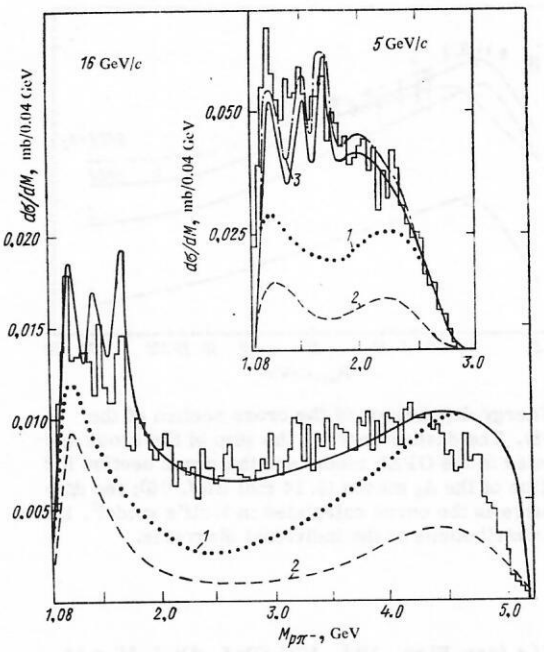

FIG. 24. Distribution with respect to the mass of the $p\pi^-$ pair in the reaction (38). 1) Total contribution of background combinations; 2) contribution of the $\pi^- p$ combination of the diagram (39b); 3) allowance for production of the A_2 meson.

In the OPE model, the reactions (38) correspond to the two diagrams[8)]

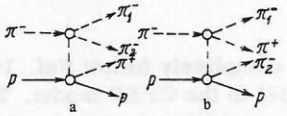

(39)

The amplitude corresponding to the diagram (39b) has been obtained above. Similarly, one can obtain the amplitude corresponding to the diagram (39a). The cross section of the reaction (38) can be calculated by squaring the amplitudes corresponding to the diagram (39) and ignoring their interference.

The energy dependence of the reaction (38) is shown in Fig. 20. Note that the flattening of the cross section at high energies is due to the presence of the vacuum poles in the $\pi\pi$ and πN scattering blocks. The asymptotic value of the cross section of the reaction (38) depends strongly on the limiting value of the $\pi\pi$ scattering cross section, which itself is known with large uncertainty. For the Regge parametrization of the $\pi\pi$ scattering amplitudes carried out in Ref. 12 and used in our calculations here, the asymptotic value of the $\pi\pi$ scattering cross section was taken equal to 12 mb.

The distributions with respect to the effective masses of the $\pi^+\pi^-$, $\pi^-\pi^-$, $p\pi^+$, $p\pi^-$, and $\pi^+\pi^-\pi^-$ combinations at 5 GeV/c (Refs. 16 and 26) and 16 GeV/c (Ref. 27) are compared with the calculated distributions in Figs. 21–25. In the theoretical distributions at 5 GeV/c allowance has been made for production of the A_2 meson (0.14 mb). In calculating its contribution, we assumed that it corresponds to a resonance in the $\pi^+\pi^-\pi^-$ system with quantum numbers 2^+, width 0.1 GeV, mass 1.31 GeV, and main decay channel to the $\rho^0\pi^-$ system. We shall now discuss in detail each of the distributions.

$M_{\pi^+\pi^-}$. The two resonances in this system (the ρ and f mesons) are well reproduced by the model and are contained in the $\pi_1^-\pi^+$ combination of the diagram (39b). The shoulder in the region of 0.5 GeV is the result of background combinations: the $\pi_2^-\pi^+$ diagram (39b) and the contribution of the diagram (39a).

$M_{\pi^-\pi^-}$. The contribution of the diagram (39b) (3) has a sharp peak around 0.5 GeV. The A_2 meson makes the main contribution in the region 0.5–1 GeV (the difference between curves 1 and 2) and significantly improves the description of the experimental data in this region.

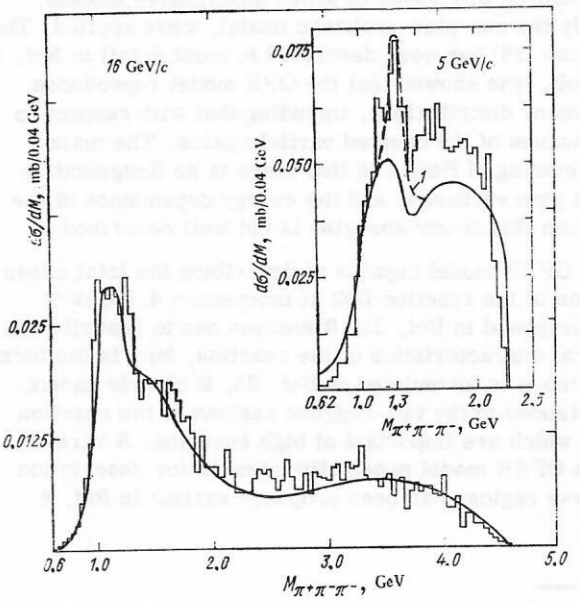

FIG. 25. Distribution with respect to the mass of the $\pi^+\pi^-\pi^-$ system in the reaction (38). 1) Allowance for the production of the A_2 meson.

[8)]Two other diagrams are obtained by transposing the two identical π^- mesons.

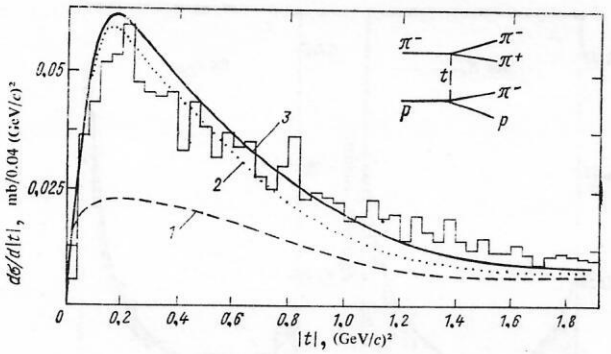

FIG. 26. Distribution with respect to the square of the momentum transferred to the $\pi^+\pi^-$ system in the reaction (38) at momentum 5 GeV/c. 1) The total contribution of the background combinations; 2) the result of calculation in the OPER model; 3) the result of calculation with allowance for production of the A_2 meson.

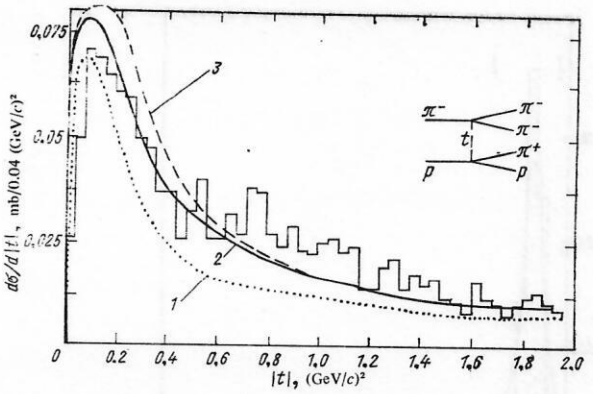

FIG. 27. Distribution with respect to the square of the momentum transferred to the $\pi^-\pi^-$ ($p\pi^+$) system in the reaction (38) at momentum 5 GeV/c. 1) Total contribution of the background combinations; 2) result of calculation in the OPER model; 3) with allowance for production of the A_2 meson.

At momentum 16 GeV/c, the OPER model without allowance for the A_2 meson gives a good description of the experimental data.

$M_{p\pi^+}$. The resonance peak $\Delta^{++}(1236)$ is contained in the contribution of the diagram (39a); the background curve 1 corresponding to the contribution of the diagram (39b) has a peak in the region of the isobar. It can be seen from a comparison of the distributions at 5 and 16 GeV/c that the relative contribution of the background in the region of the isobar decreases with increasing energy.

$M_{p\pi^-}$. The contribution of the $\pi_2^- p$ combination of the diagram (39b) contains three resonance maxima: $\Delta^0(1236)$, $N^*(1520)$, and $N^*(1690)$. The experiment only hints at the resonances $N^*(1520)$ and $N^*(1690)$. The statistics must be improved if they are to be singled out more clearly. The contributions of the diagram (39a) and the $\pi_1^- p$ combination of the diagram (39b) have a sharp near-threshold peak (1), which to a considerable extent determines the cross section in the region of the $\Delta^0(1236)$ isobar.

$M_{\pi^-\pi^+\pi^-}$. The model reproduces well the peak in the region of the so-called A_1 meson (1.1–1.2 GeV). This peak arises in the same way as the peak previously discussed in the $p\pi^+\pi^-$ system around 1.7 GeV in the reaction $pp \to pp\pi^+\pi^-$. We emphasize that both peaks are described quantitatively for one and the same set of parameters. The deviation of the theoretical curve from the experimental histogram in this figure in the region $M_{3\pi} > 1.5$ GeV is possibly due to the presence of other mechanisms for the reaction (38) at low energies. Note the presence of the shoulder in the theoretical curve in the region of the A_3 meson (1.6–1.7 GeV) at 16 GeV/c.

The distributions with respect to the squares of the momenta transferred to the $\pi^+\pi^-(p\pi^-)$ and $\pi^-\pi^-(p\pi^+)$ systems (at 5 GeV/c) are shown in Figs. 26 and 27, from which it can be seen that the model gives somewhat more strongly peaked curves than experiment.

Curve 1 in Fig. 26 is the contribution of the diagram (39a), and in Fig. 27 it is the contribution of the diagram (39b). Both curves are background curves for the extrapolation of the experimental data to the position of the pion pole of the diagrams (39a) and (39b). It can be seen from the figures that the growth of the background curves in the region of small momentum transfers (especially in Fig. 27) can make the extrapolation much more difficult.

The predictions of the model are compared with the distributions with respect to the longitudinal momenta of the proton and the pions at momentum 5 GeV/c in Fig. 28. The cross sections for the positively charged particles are plotted upward and those for the negatively charged particles downward from the horizontal axis. The hatched histogram corresponds to the distribution of the total charge. The model with allowance for the contribution from the decay of the A_2 meson satisfactorily describes the experimental data.

Description of the regions of small momentum transfers in the reaction $\pi^- p \to \pi^-\pi^-\pi^+ p$. *Study of the reaction mechanism.* Turning to a more detailed description of

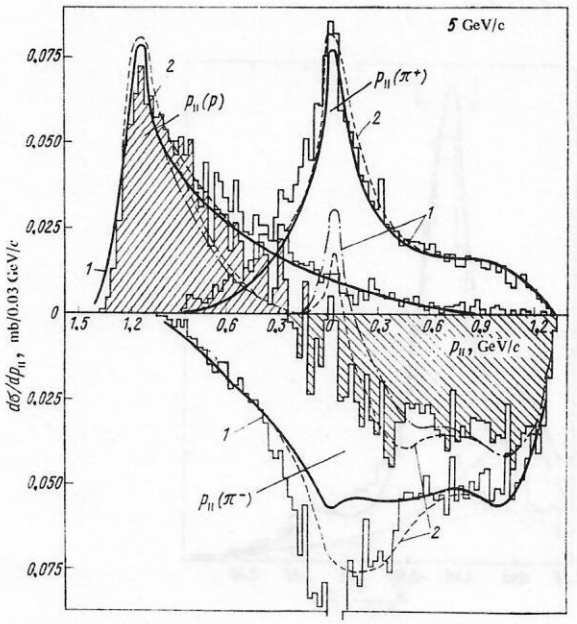

FIG. 28. Distributions with respect to the longitudinal momenta of all particles in the reaction (38) at momentum 5 GeV/c. 1) Result of calculation in the OPER model; 2) in the OPER model with allowance for the contribution from the decay of the A_2 meson.

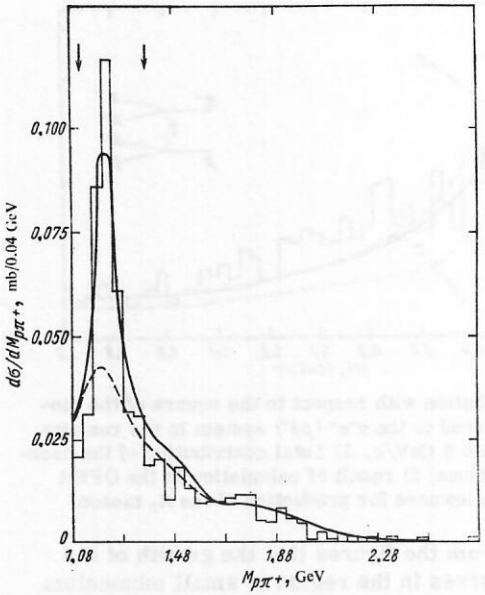

FIG. 29. Distribution with respect to the mass of the $p\pi^+$ system when it is peripherally produced ($|t| < 0.4$ GeV^2) in the reaction (38) at momentum 5 GeV/c. The dashed curve is the contribution of the diagram (39b).

the reaction (38), we shall, as in the description of the reaction $pp \to pp\pi^+\pi^+$, be interested primarily in the regions near the position of the poles of the individual diagrams (39). For the diagram (39a) in the experiment of Ref. 16 at momentum 5 GeV/c the corresponding region is determined by the condition that the momentum transferred to the $p\pi^+(\pi^-\pi^-)$ system be small:

$$|t|_{p\pi^+} < 0.4 \text{ GeV}^2, \tag{40}$$

and for the diagram (39b) it is determined by the condition that the momentum transferred to the $\pi^+\pi^-(p\pi^-)$ system be small:

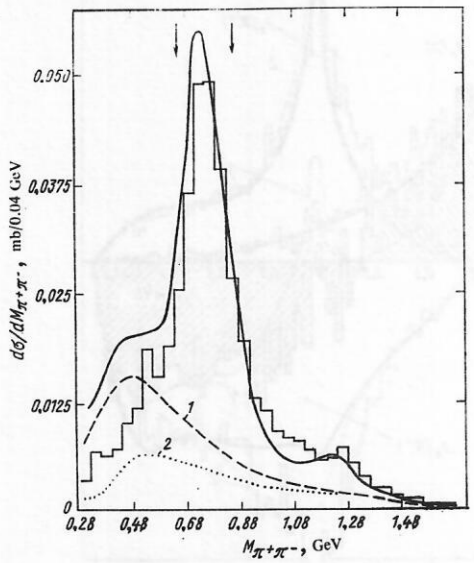

FIG. 30. Distribution with respect to the mass of the $\pi^+\pi^-$ pair when it is produced peripherally ($|t| < 0.4$ GeV^2) in the reaction (38) at momentum 5 GeV/c. 1) Total contribution of the background combinations of diagrams (39a) and (39b); 2) contribution of the diagram (39a).

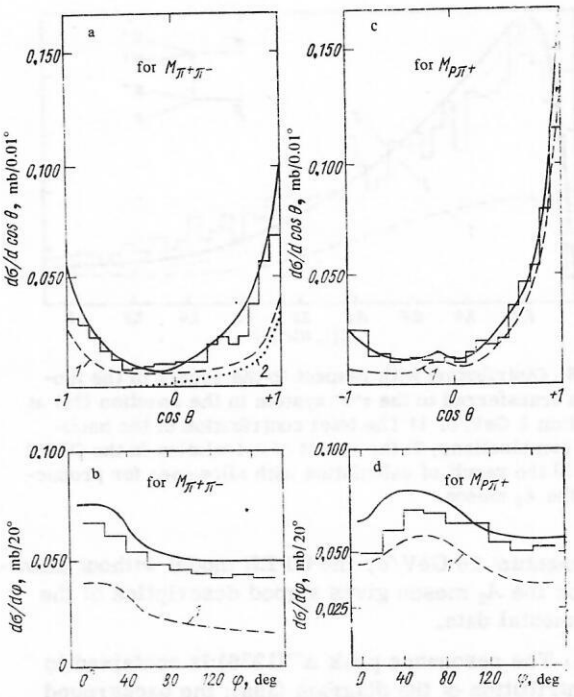

FIG. 31. Distributions with respect to the angular variables of the decay of the $\pi^+\pi^-$ (a and b) and $p\pi^+$ (c and d) systems when they are peripherally produced ($|t| < 0.4$ GeV^2) in their center-of-mass systems in the reaction (38) at momentum 5 GeV/c. 1) Total contribution of background combinations; 2) contribution of the diagram (39a).

$$|t|_{\pi^+\pi^-} < 0.4 \text{ GeV}^2. \tag{41}$$

The distribution with respect to the mass of the $p\pi^+$ system subject to the restriction (40) is shown in Fig. 29. The contribution of the diagram (39b) is predominant everywhere, except in the region of the isobar $\Delta^{++}(1236)$. A similar distribution with respect to the mass of the $\pi^+\pi^-$ system subject to the restriction (41) is shown in Fig. 30. The total contribution of the $\pi_2^-\pi^+$ combination of the diagram (39b) and the contribution of the diagram (39a) has a maximum in the region of 0.45—0.5 GeV and is apparently overestimated in the model. However, bearing in mind that in this region all amplitudes corresponding to different combinations of $\pi^+\pi_i^-$ pairs make an appreciable contribution, we believe that allowance for the interference of these amplitudes will reduce the difference between the theoretical and the experimental data.

The distributions with respect to the cosine of the polar angle and the azimuthal angle in the center-of-mass system of the $\pi^+\pi^-$ pair under the restriction (41) are shown in Figs. 31a and 31b. The analogous distributions in the center-of-mass system of the $p\pi^+$ pair under the restriction (40) are shown in Figs. 31c and 31d. The angles are defined in the Gottfried—Jackson coordinate system in the same way as the angles θ^+, φ^+ (θ^-, φ^-) defined earlier. Let us discuss in more detail each of the distributions in Fig. 31.

$\theta_{\pi^+\pi^-}$. The contribution of the background combination $\pi_2^-\pi^+$ of the diagram (39b) is concentrated in the backward cone, whereas the contribution of the diagram (39a) is concentrated in the forward cone. The resultant

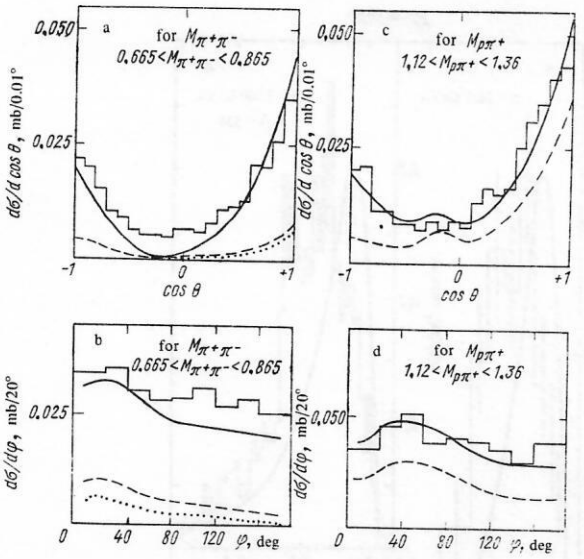

FIG. 32. The same as Fig. 31 with an additional restriction on the masses of the $\pi^+\pi^-$ and $p\pi^+$ systems.

distribution has virtually the same forward-backward asymmetry as the contribution of the main combination, which is equal to the difference between the continuous and the dashed curve in Fig. 31a.

$\varphi_{\pi^+\pi^-}$. The main combination is practically isotropic—the exchange of a Reggeized pion at this energy behaves like the exchange of an elementary pion. The contribution of the $\pi_2^-\pi^+$ combination of the diagram (39b) is also isotropic. The contribution of the diagram (39a) determines the asymmetry of the distribution.

$\theta_{p\pi^+}$. The background combination [the contribution of the diagram (39b)] is predominant and responsible for the large symmetry of the distribution.

$\varphi_{p\pi^+}$. As in the $\varphi_{\pi^+\pi^-}$ case, the main combination is isotropic. The background combination has a characteristic peak around 60°. Note that, as one would expect, the contribution of the background combination in this reaction is qualitatively the same as the analogous contribution in the reaction $pp \to p\pi^-\Delta\Delta^{++}(1236)$, which is indicated in Fig. 14 by the dashed curve.

Figure 32 contains distributions analogous to those of Fig. 31, but with additional selection with respect to the mass of the $\pi^+\pi^-$ system in the region of the ρ meson (a, b) and with respect to the mass of the $p\pi^+$ system in the region of the Δ^{++} isobar (c, d). The contribution of the background combinations is most strongly changed. It is reduced by 15% in the region of the ρ meson and by up to 60% in the region of the isobar. However, the general nature of the distributions is little changed. Curves analogous to those of Figs. 32a and 32b (without separation of the contribution from different diagrams) were obtained in Refs. 25, 28, and 29 in an analysis of the reaction (38) at momenta 4.5 and 3.9 GeV/c in models similar to those used by us at low energies.

In the case of peripheral production of a system of two pions in a pion beam the most dangerous competitor of pion exchange is evidently the exchange of a

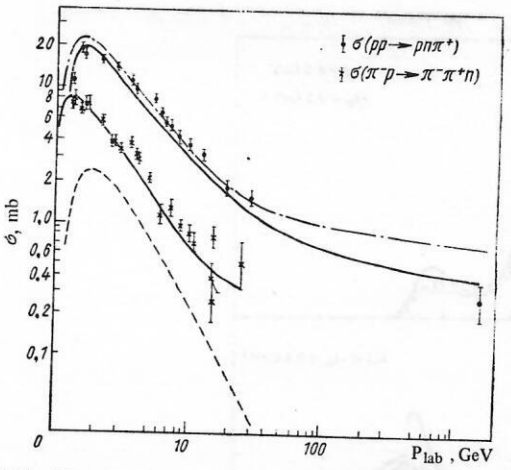

FIG. 33. Energy dependence of the cross sections of the reactions $pp \to pn\pi^+$ and $\pi^-p \to \pi^-\pi^+n$. The dashed curve is the contribution of the diagrams with charge exchange (43c and 43d); the dot-dash-dot curve is the old variant of the model; the continuous curve is the new variant.

trajectory with natural spin-parity relation and negative G parity (the A_2 trajectory). One can show that the angular distributions in the center-of-mass system of the pion pair in this case must be proportional to $\sin^2(\theta_{\pi^+\pi^-})\sin^2(\varphi_{\pi^+\pi^-})$. The experimental distributions in Figs. 31a, 31b, 32a, and 32b are inconsistent with this function. An estimate of its possible contribution to these distributions showed that it is not greater than 10%.

Thus, one-pion exchange is predominant in the production of the $\pi^+\pi^-$ and $p\pi^+$ systems in the region of small momentum transfers [$|t| < 0.4$ (GeV/c)^2], just as it is in the production of $p\pi$ pairs in the reaction $pp \to pp\pi^+\pi^-$.

Description of the process $pp \to p\pi^+n$

The reaction

$$pp \to p\pi^+n \qquad (42)$$

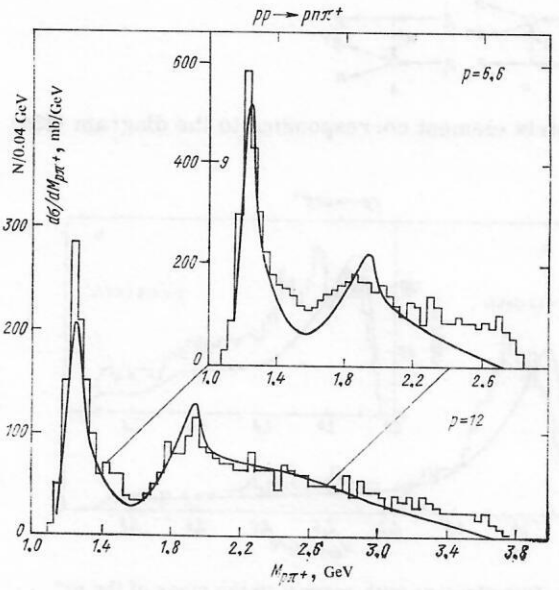

FIG. 34. Distributions with respect to the mass of the $p\pi^+$ system in the reaction (42).

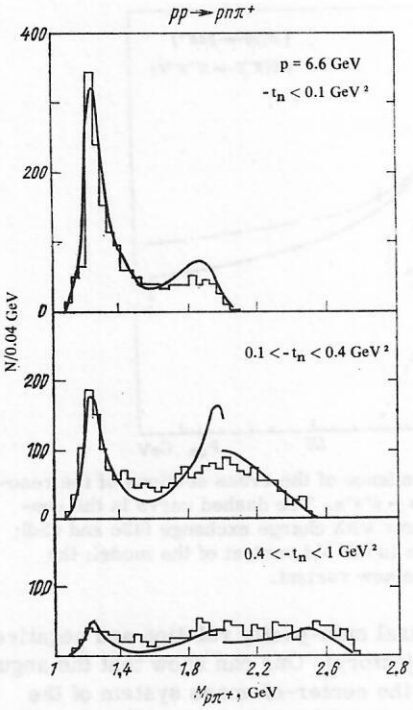

FIG. 35. The same as in Fig. 34 for different momenta t_n transferred to the $p\pi^+$ system.

is basic for finding the last unknown parameter R_1^2, which describes the dependence on the departure from the mass shell of the exchanged pion in the one-block graphs. In all calculations, we take $R_1^2 = 1.9$ GeV^{-2}.

We shall analyze the experimental data on the reaction (42) in the new variant of the model (see above) by means of the diagrams

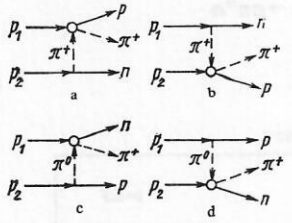

(43)

The matrix element corresponding to the diagram (43a)

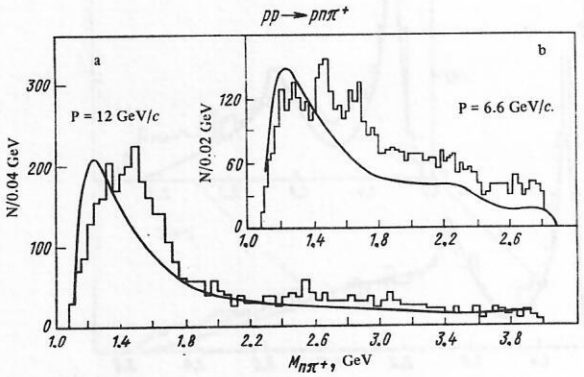

FIG. 36. Distributions with respect to the mass of the $n\pi^+$ system in the reaction (42) at the momenta 6.6, 12, 28.5 ($0.06 < t_p < 1$), and 1500 GeV($|t_p| > 0.05$ GeV^2).

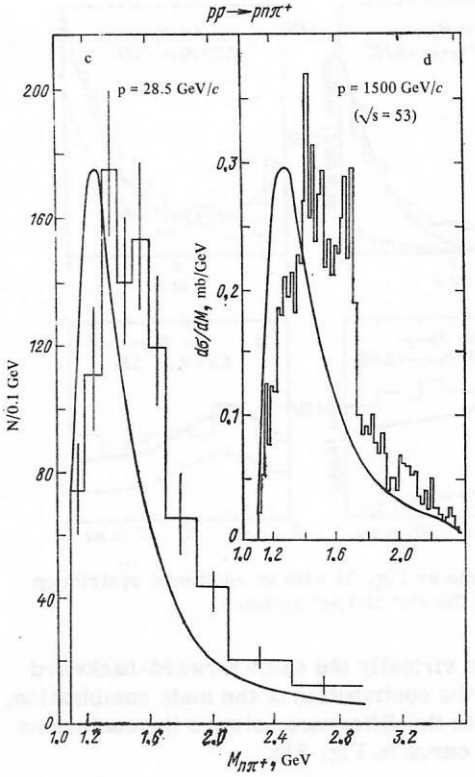

FIG. 36c and 36d.

has been given above. The amplitudes corresponding to the remaining graphs can be expressed similarly. We shall obtain the cross section of the reaction (42), summed over the spins of the nucleons, by adding the squares of the moduli of the corresponding amplitudes. There is no interference between the diagrams (43a) and (43d) [(43b) and (43c)] because of the different spin structure of the amplitudes, and the remaining interference terms are small because the ranges of variation of the momentum transfers in which the various diagrams are large do not overlap.

The energy dependence of the reaction cross section (42) is shown in Fig. 33, from which it can be seen that at low and medium energies ($p_{1ab} < 30$ GeV/c) the two variants differ little. The experiment made in colliding rings[30] at $\sqrt{s} = 53$ GeV ($p_{1ab} \approx 1500$ GeV/c) is critical. The new variant of the model gives a cross section at this energy which coincides with the upper limit of the error of the experimental value, whereas the cross section obtained in the old variant exceeds it by about 2.5 times. The total cross section, as usual, flattens out at higher energy, this being due to the contribution of the vacuum pole to the block of virtual $\pi^+ p$ scattering. The relative contribution of the diagrams with charge exchange decreases strongly with increasing energy, reaching the maximal value (about 15%) at low energies.

The distribution with respect to the mass $M_{p\pi^+}$ at 6.6 GeV/c (Ref. 31) and 12 GeV/c (Ref. 32) is shown in Fig. 34. The theoretical curves correspond to the cross section of elastic $\pi^+ p$ scattering and contain the two resonances $\Delta^{++}(1236)$ and $\Delta^{++}(1960)$. The small value of the theoretical cross section for production of the isobar $\Delta^{++}(1236)$ at the momentum 12 GeV/c is evidently due to the increased contribution at higher energies of

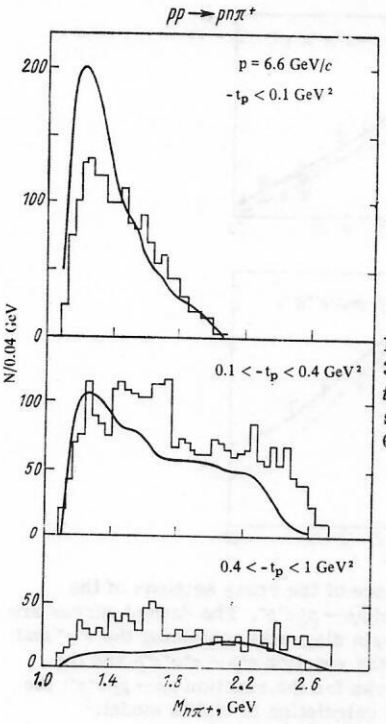

FIG. 37. The same as Fig. 36 for different momenta t_p transferred to the $n\pi^+$ system and momentum 6.6 GeV/c.

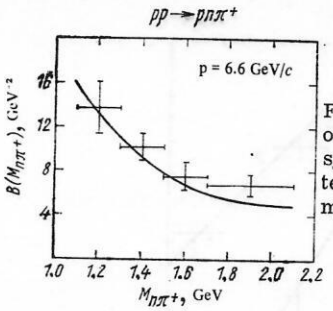

FIG. 38. Dependence of the slope of the peak for production of $n\pi^+$ system on the mass of the system in the reaction (42) at momentum 6.6 GeV/c.

the ρ and A_2 trajectories, which lies above the pion trajectory on the Chew–Frautschi plane. Figure 35 shows the same distribution under three restrictions on the momentum transferred to the $p\pi^+$ system: $|t_{p\pi^+}| < 0.1$ GeV^2, $0.1 < |t_{p\pi^+}| < 0.4$ GeV^2, $0.4 < |t_{p\pi^+}| < 1$ GeV^2. It can be seen from the figure that the rate of decrease of the cross section with increasing momentum transfer decreases as the mass of the $p\pi^+$ system increases. Such a dependence follows directly from the expression (21) for the form factor F_1. The effective argument of the exponential in this expression decreases logarithmically with increasing mass of the block (about as $\ln S_1$). The discontinuity in the theoretical distribution at the mass 2 GeV is due to the different parametrization of the πN elastic scattering amplitude at low and high energies (see the Appendix).

The distribution with respect to the mass of the $p\pi^+$ system is shown in Figs. 36a and 36b [$p = 12$ GeV/c (Ref. 31) and 6.6 GeV/c (Ref. 32)] and in Figs. 36c and 36d [$p = 28.5$ GeV/c, $0.2 < |t_{n\pi^+}| < 0.8$ (GeV/c)^2 (Ref. 33)]; $\sqrt{s} = 53$, 0.05 GeV$^2 < |t_{n\pi^+}|$ (Ref. 30).[9] The theoretical curves have a near-threshold peak (in the region of 1.2–1.3 GeV). Its origin is the same as that of the peak in the $p\pi^+\pi^-$ system in the reaction $pp \to pp\pi^+\pi^-$ in the region of $M_{p\pi^+\pi^-} \approx 1.7$ GeV and the peak known as the A_1 meson in the $\pi^-\pi^-\pi^+$ system in the reaction $\pi^- p \to \pi^-\pi^+\pi^- p$, both of which were discussed earlier. Besides this near-threshold peak, the experiment indicated production of isobars in the region $M_{n\pi^+} \sim 1.4$–1.7 GeV not contained in the model, their relative contribution to the cross section not dying out with increasing energy. The change in the spectrum with respect to the mass $M_{n\pi^+}$ with increasing momentum transfer is given in Fig. 37, which shows that the near-threshold peak is produced essentially for $|t_p| < 0.1$ (GeV/c)^2, whereas the resonances are at large momentum transfers. Representing the dependence of the distribution with respect to the mass $M_{n\pi^+}$ on the momentum transfer in the exponential form $d^2\sigma/dt\,dM_{n\pi^+} \sim \exp[B(M_{n\pi^+})t]$, we are interested in $B(M_{n\pi^+})$. The experimental value of this quantity is compared with the theoretically calculated values at momentum 6.6 GeV/c in Fig. 38. Despite the strong decrease of the argument with increasing mass (by about 3 times), there is good agreement between experiment and theory.

The distributions with respect to the square of the momentum transferred from the initial to the final proton, integrated over the whole range of masses of the $n\pi^+$ system, are shown in Fig. 39. There is a strong narrowing of the cone with increasing energy, this being more pronounced in the model than experimentally. This, in particular, is due to our taking $\alpha'_p = 0.5$ GeV^{-2} for the slope of the vacuum pole when parametrizing

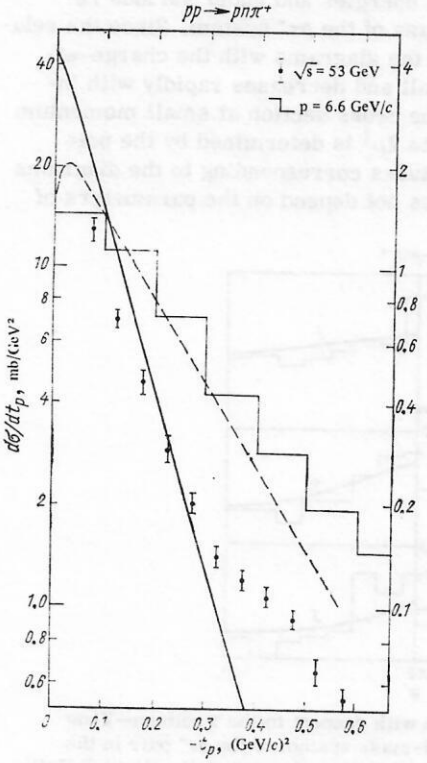

FIG. 39. Distributions with respect to the square of the momentum transferred to the $n\pi^+$ system in the reaction (42). The left-hand scale refers to the data at 6.6 GeV/c; the right-hand one, to the energy $\sqrt{s} = 53$ GeV.

[9] The theoretical curve is normalized to have the same area as the experimental histogram.

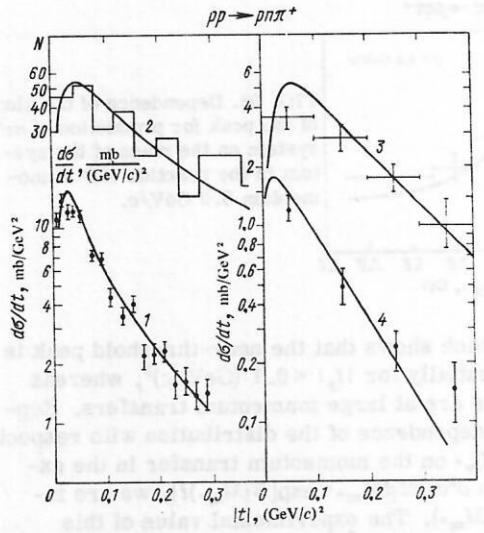

FIG. 40. Distributions with respect to the square of the momentum transferred to the $p\pi^+$ system in the reaction (42). 1) $p = 6.6$ GeV/c, $M_{\pi^+p} < 1.4$ GeV (Ref. 40); 2) $p = 28.5$ GeV/c, $M_{p\pi^+} > 2$ GeV; $0.06 < |t_p| < 1$ GeV^2 (Ref. 4); 3) $p = 10$ GeV/c, $M_{p\pi^+} > 1.325$ GeV (Ref. 41); 4) $p = 19$ GeV/c, $1.54 < M_{p\pi^+} < 2.05$ GeV (Ref. 42).

the πN scattering amplitude (see the Appendix), whereas the most recent experiments[34] at energies above 100 GeV have given $\alpha'_p = 0.2-0.3$ GeV^{-2}.

From the point of view of testing and formulating the model, an important distribution is that with respect to the square of the momentum t_n transferred from the proton to the neutron. This distribution is shown in Fig. 40 for several energies and under various restrictions on the mass of the $p\pi^+$ system. Since the relative contribution of the diagrams with the charge-exchange block is small and decreases rapidly with increasing energy, the cross section at small momentum transfers $|t_n| = \mu^2$ to $2\mu^2$ is determined by the pole values of the amplitudes corresponding to the diagrams (43a) and (43b), does not depend on the parameters of

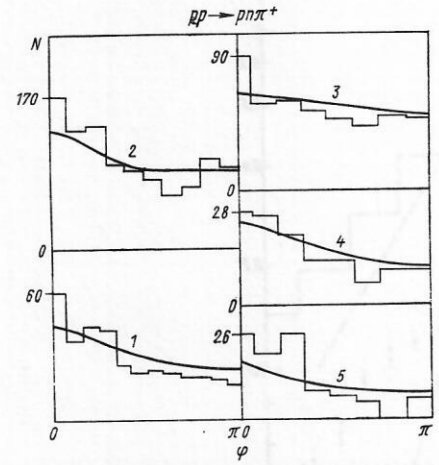

FIG. 41. Distribution with respect to the Treiman–Yang angle in the center-of-mass system of the $p\pi^+$ pair in the reaction (42). 1) $p = 28.5$ GeV/c, $M_{p\pi^+} > 2$ GeV, $|t| < 0.8$ GeV^2, $0.06 < |t_p| < 1$ GeV^2 (Ref. 4); 2) $p = 7$ GeV/c (Ref. 43); 3) $p = 7$ GeV/c, $0 < |t| < 0.2$ GeV^2; 4) $p = 7$ GeV/c; $0.2 < |t| < 0.4$ GeV^2; 5) $p = 7$ GeV/c, $0.2 < |t| < 0.4$ GeV^2 (the theoretical curve is plotted on a 1:3 scale) (Ref. 43).

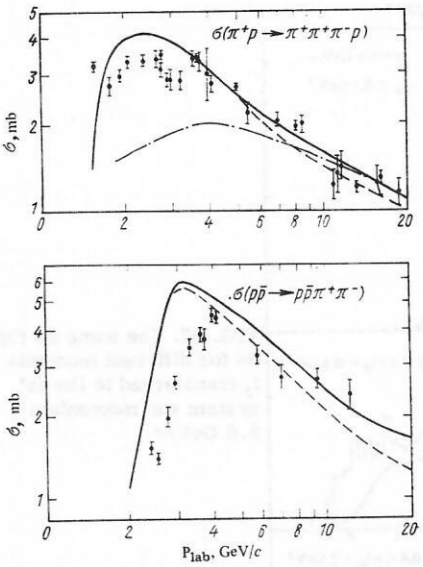

FIG. 42. Energy dependence of the cross sections of the reactions $\pi^+p \to \pi^+\pi^+\pi^-p$ and $\bar{p}p \to pp\pi^+\pi^-$. The dashed curves are the contributions of the main diagrams containing the $\pi^+\pi^-$ and π^+p scattering blocks for the reaction $\pi^+p \to \pi^+\pi^+\pi^-p$ and the π^+p and $\pi^-\bar{p}$ scattering blocks for the reaction $p\bar{p} \to p\bar{p}\pi^+\pi^-$; the dot-dash-dot curve is the calculation in Wolf's model.[3]

the model, and is predicted absolutely. On the other hand, the behavior of the cross section at large momentum transfers depends most directly on the free parameter R_1^2 of the model and makes possible its determination with the best accuracy.

A characteristic feature of the experimental data at high energy is the appreciable asymmetry in the distribution with respect to the Treiman–Yang azimuthal angle in the π^+p rest frame. This angle is defined like the angle φ^+ in Eq. (33). The distributions with respect to this quantity are shown in Fig. 41. In the model, the observed asymmetry is due to the factor $(k_\perp^2 + \mu^2)^{\alpha_\pi(t)}$ in the form factor (22). Moreover, in complete agreement with this expression, the asymmetry increases with increasing momentum transfer (see Fig. 41).

3. PROCESSES NOT CONSIDERED IN THIS PAPER

Besides the detailed description of the above processes in this present variant of the OPER model, the energy dependence of the cross sections of the following processes were calculated without additional free parameters:

$$\pi^-p \to \pi^-\pi^+n; \tag{44}$$

$$\pi^+p \to \pi^+\pi^+\pi^-p; \tag{45}$$

$$p\bar{p} \to p\bar{p}\pi^+\pi^-. \tag{46}$$

The cross section of the reaction (44) is shown in Fig. 33, and the cross section of the reactions (45) and (46) in Fig. 42. The reaction (44) is described in detail in Refs. 12 and 13 in the old formulation of the model (see above). In these papers it was shown that at momenta $p \leq 25$ GeV/c the model gives a good quantitative description of the basic characteristics of this reaction: the distributions with respect to the masses of the $\pi^+\pi^-$, π^-n, n^+p pairs; the distributions with respect to the momentum transfers, and the angular distributions in the center-of-mass system of the $\pi^+\pi^-$ pair. We recall

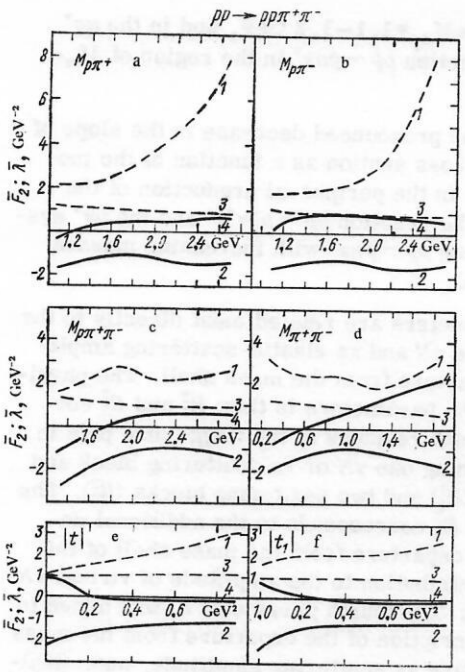

FIG. 43. Characteristic distributions of the mean values of the form factor F_2 (F_R and F_p, curve 1 and 3) and the effective argument of the exponential in the form factor F_2 (λ_R and λ_p, curves 2 and 4).

that at these energies there is no reason to expect a difference between the descriptions of the reaction (44) in the old and new formulations of the model.

The reactions (45) and (46) have not been considered in detail in the OPER model, although in the majority of experimental investigations individual characteristics of these processes have been described by various modifications of the OPE model. These reactions are different from all those considered earlier because the quasi-two-particle regions $\pi^+p \to \rho^0\Delta^{++}$ and $p\bar{p} \to \Delta^{++}\bar{\Delta}^{++}$ make large contributions to the cross sections of these processes. The quasi-two-particle region is the furthest from the region of three-reggeon kinematics. As a result, in the processes (45) and (46) one can, especially at low energies, expect discrepancies between the theoretical calculations and the experimental data. In particular, this is due to the poor description of the cross section of the reaction (48) at momenta $p_{1ab} < 4$ GeV/c.

We note finally that the experimental and theoretical investigations of the reaction (44), and also the other processes of single-pion creation, have shown that one-pion exchange dominates only in the reactions in which there is charge exchange of a proton (or neutron) of the target. Otherwise, i.e., in processes of the type $\pi^\pm p \to \pi^\pm\pi^0 p$, $pp \to p\pi^0 p$, etc, the one-pion-exchange contribution does not exceed that of the trajectories with the natural spin-parity relation (A_2, ρ, ω, p'). In contrast to this, exchange of the pion trajectory is predominant in all the investigated two-pion-production processes.

4. NUMERICAL ANALYSIS OF THE FORM FACTORS

As can be seen from Eqs. (17b) and (22), the form factors F_2 and F_1 are fairly complicated functions of different kinematic variables, which makes difficult their quantitative analysis. Here we carry out a numerical analysis of the more complicated one, F_2. We shall study F_2 and the effective argument λ of the exponential in (17b). For the contribution of the vacuum pole to the $\pi\pi$ and πN scattering blocks there is an additional dependence on the departure from the mass shell t, which is given in (17b), and we shall therefore analyze the form factor in two regions: at low energy, at which the vacuum poles are not important, and at high energies, where we shall use an amplitude containing only the vacuum pole in one of the blocks. We denote by λ_R the argument of the exponential in (17b):

$$\lambda_R = R_2^2 + \alpha_\pi' \ln\left(\frac{s}{s_0}\frac{\varkappa_1^2}{s_1}\frac{\varkappa_2^2}{s_2}\right). \tag{47}$$

We also introduce

$$\lambda_p = \lambda_R + R_p^2 \quad F_R = \exp[\lambda_R(t-\mu^2)]; \tag{48}$$

$$F_p = \exp[\lambda_p(t-\mu^2)]. \tag{49}$$

It is of interest to calculate the mean values of the form factors and the arguments:

$$\bar{F}_i = \int |\overline{M}|^2 F_i\, d\tau \Big/ \int |\overline{M}|^2 d\tau; \tag{50}$$

$$\bar{\lambda}_i = \int |\overline{M}|^2 \lambda_i\, d\tau \Big/ \int |\overline{M}|^2 d\tau, \quad i = R,\ P. \tag{51}$$

The integration in (50) and (51) is over the whole phase space of the reaction (7). The values of $\bar{F}_R$ and $\bar{\lambda}_R$ are calculated at the momentum 6.6 GeV/c, and the amplitude corresponding to the diagram (6a) is taken as the matrix element. The values of $\bar{F}_p$ and $\bar{\lambda}_p$ are calculated at the momentum 205 GeV/c with the same matrix element, only the contribution of the vacuum pole being retained in the amplitude of π^-p elastic scattering, corresponding to the lower block. For the mean values, we obtain $\bar{F}_R = 2.46$, $\bar{\lambda}_R = -1.33$ GeV^{-2}, $\bar{F}_p = 1.04$, $\bar{\lambda}_p = 0.17$ GeV^{-2}.

Besides the integral mean values, it is of interest to obtain the distributions of these quantities as functions of the same variables that the differential cross section of the reaction (7) was studied as a function of: the masses of the $p\pi^+$, $p\pi^-$, $\pi^+\pi^-$ pairs, the mass of the $p\pi^+\pi^-$ system, and the momentum transfers t and t_p. These distributions are shown in Fig. 43. By the distribution with respect to t we understand, for example, the integral

$$\bar{F}_i(t) = \frac{\int |\overline{M}|^2 F_i\, d\tau'}{\int |\overline{M}|^2 d\tau'}\,\bar{\lambda}_i(t) = \frac{\int |\overline{M}|^2 \lambda_i\, d\tau'}{\int |\overline{M}|^2 d\tau'}, \quad i = R,\ P. \tag{52}$$

In (52), the integration is over the whole phase space of the reaction (1) for a fixed value of t.

Analyzing the results, we note first of all that at low energies the form factors increase everywhere, whereas at high energy the form factor is everywhere near unity. Increasing form factors are necessary to describe the total cross section of the two-block reactions and they are a distinctive feature of the OPER model. It should be noted that increasing form factors could also appear in models of the type used by Wolf[3] because of factors which increase with respect to t and take into account the departure from the mass shell of the partial-wave πN elastic-scattering amplitudes:

$$f_l(t) = (q(t)/q(\mu^2))^l f_l(\mu^2); \tag{53}$$

here, $q(\mu^2)(q(t))$ is the three-momentum of the pion on (respectively, off) the pion mass shell.

Let us discuss some of the details of Fig. 43. The strong increase in F_2 at large masses in Figs. 43a and 43b corresponds to the increase in this region of the mean momentum transfers. The decrease of the arguments λ_R and λ_p in the threshold region in Figs. 43c and 43d corresponds to the appearance of kinematic peaks in the region of 1.7 GeV with the respect to the mass of the $p\pi^+\pi^-$ system and in the region 0.5 GeV with respect to the mass of the $\pi^+\pi^-$ system (see Figs. 7–19). The value of $\bar{F}_R(t)$ increases almost linearly with increasing $|t|$, the argument $\lambda_R(t)$ varying slowly. It is remarkable that the form factor $\bar{F}_p(t)$ is equal to unity and the argument $\bar{\lambda}_p(t)$ to zero in a wide range of the momentum transfers t and t_p. This condition was not fed into the model and does not in any way follow from the general expression for the form factor.

Because of the appreciable value of the radius R_1^2, the form factor F_1 is on the average decreasing ($\bar{F}_1 < 1$). At the same time, its basic qualitative features must be the same as F_2, as can be seen from (17b) and (22).

Finally, let us note the following. The form factors were chosen rather arbitrarily in the form (17b) and (22) without sufficient theoretical justification. One could perhaps construct form factors using quite different functions. However, if the amplitudes with such form factors are to describe the experimental data satisfactorily, the averaged values of the form factors will satisfy the same general dependences as the corresponding curves in Fig. 43.

CONCLUSIONS

The OPER model has here been applied to the reactions in which one or two mesons are produced in πN and NN collisions. The model depends on five free parameters, which have been determined by describing the reactions

$$pp \to pp\pi^+\pi^-,\ \pi^-p \to \pi^-\pi^-\pi^+p,\ pp \to pn\pi^+. \tag{54}$$

In this model with fixed values of the parameters we have:

1) described the energy dependence of the reactions (54) and also the reactions $\pi^-p \to \pi^-\pi^+n$, $\pi^+p \to \pi^+\pi^-\pi^+p$, $\bar{p}p \to \bar{p}p\pi^+\pi^-$ at energies above a few GeV;

2) described the general characteristics of the reactions (54), namely, the distributions with respect to the two-particle masses, with respect to the three-particle masses, and with respect to the squares of the momentum transfers;

3) described the angular distributions in the center-of-mass systems of the πp or $\pi\pi$ particle pairs when they are produced peripherally. In particular, we have described the asymmetry with respect to the Treiman–Yang azimuthal angle in these systems;

4) described qualitatively the apperance of the near-threshold peaks (Deck effect) in the $p\pi^+\pi^-$ system in the reaction $pp \to pp\pi^+\pi^-$ in the region of $M_{p\pi^+\pi^-} \approx 1.7$ GeV, in the $\pi^+\pi^-\pi^-$ system in the reaction $\pi^-p \to \pi^-\pi^+\pi^-p$ in the region of $M_{\pi^+\pi^-\pi^-} \approx M_{A_1} \approx 1.1$–$1.2$ GeV, and in the $n\pi^+$ system in the reaction $pp \to pn\pi^+$ in the region of $M_{n\pi^+} \approx 1.2$–1.3 GeV;

5) described the pronounced decrease in the slope of the differential cross section as a function of the momentum transfer in the peripheral production of the $p\pi^+\pi^-$ system in the reaction $pp \to pp\pi^+\pi^-$ and the $n\pi^+$ system in the reaction $pp \to pn\pi^+$ with increasing masses of these systems.

The free parameters are related most directly to the dependence of the πN and $\pi\pi$ elastic-scattering amplitudes on the departure from the mass shell. The physical meaning of the parameters is this: R_1^2 and R_2^2 correspond to the total residues of the Regge pion pole in diagrams containing one πN or $\pi\pi$ scattering block and the $NN\pi$ vertex (R_1^2) and two scattering blocks (R_2^2). The third parameter R_p^2 corresponds to the additional dependence on the departure from the mass shell of the vacuum-pole contribution to the amplitude of virtual πN or $\pi\pi$ scattering. The fourth parameter c_ρ was added to improve the description of the departure from the mass shell of the P-wave $\pi\pi$ scattering amplitude, and, finally, by means of the fifth parameter c the form factors F_1 and F_2 found in the region of small momentum transfers were extended to the region of momentum transfers $|t| \geq 1$ $(\text{GeV}/c)^2$. The parameters R_2^2, R_p^2, c were determined from the description of the process $pp \to pp\pi^+\pi^-$, the parameter c_ρ from that of the process $\pi^-p \to \pi^-\pi^-\pi^+p$, and R_1^2 from the process $pp \to pn\pi^+$.

The only earlier attempt to describe the total cross section of the exclusive reactions

$$\pi^\mp \to \pi^\mp\pi^+\pi^-p \tag{55}$$

at different energies was undertaken in a model with exchange of an elementary pion (OPE) and with parameters determined by Wolf.[3] The result of calculation of the energy dependence of the cross sections is shown in Figs. 20 and 42 by the dot-dash-dot curves. It can be seen from the figures that this model does not describe the total cross section satisfactorily at momenta below 7–8 GeV/c.

In which region of phase space at low energies does one observe the greatest difference between the predictions of the OPER and OPE model? Now the production of resonances [ρ and f mesons and the $\Delta^{++}(1236)$ isobar] is predominant at these energies in the reactions (55), and we therefore split the phase space into two regions: A, which is the quasi-two-particle region (for example, $\pi^+p \to \rho^0\Delta^{++}$) and B, the quasi-three-particle region (for example, $\pi^+p \to \rho^0\pi^+p$). It follows from Ref. 3 and also other studies based on the OPE model that region A is satisfactorily described by the OPE model. Therefore, the two models will differ most in the quasi-three-particle regions.

The decrease of the effective radius in the form factors F_1 (22) and F_2 (17b) with increasing invariant masses of the blocks (s_1, s_2) tends to increase the cross sections in the quasi-three-particle regions in the OPER model. It follows from the way in which F_1 and F_2 were obtained that this dependence is a natural consequence of the Reggeization of the pion exchange.

TABLE A.1. Parameters of the Regge-pole parametrization of πN scattering amplitudes, GeV.

Parameter	$\alpha_i(0)$	$\alpha'_i(0)$	γ_{fi}	γ_{gi}	R_i^2
p	1.0	0.5	2.15	1.0	2.7
p'	0.5	0.5	1.54	1.0	4.3
ρ	0.5	1.0	0.264	−2.55	4.55

Further development of the model will entail its extension to exclusive processes with higher multiplicity, such as $\pi N \to (4\pi)N$ and $NN \to (3\pi)NN$, and its application to inclusive and semi-inclusive processes. First calculations of inclusive spectra of protons in the fragmentation region, and also the qualitative analysis of the spectra of other particles in NN collisions made in Ref. 15 in a variant of the model slightly different from here, produced good agreement between the theoretical calculations and the experimental data.

It is also intended that rescattering effects should be taken into account in the one-pion graphs. It is to be hoped that this can explain the observed deviations of the experimental data from the theoretical predictions and establish why processes with the production of two pions can be described better than those in which one is produced. The first explanation which springs to mind is that the amplitudes of processes with the production of one pion become zero at zero momentum transfer, whereas the amplitudes of processes with the production of two pions do not become small in this way.

I thank K. G. Boreskov, V. V. Vladimirskiĭ, A. B. Kaĭdalov, R. M. Lebedev, and K. A. Ter-Martirosyan for discussing the results in the paper. I also thank T. K. Stadnikovaya for assistance in drafting the paper.

APPENDIX

1. Parametrization of πN scattering amplitudes

To parametrize the πN scattering amplitudes, we split the complete mass range into two parts. In the region of small masses ($M_{\pi N} < 2$ GeV), in which resonance production predominates, we shall parametrize the amplitudes by means of the phase-shift analysis carried in Ref. 35. In the region of large masses ($M_{\pi N} > 2$ GeV) we shall describe the amplitude by means of the result of Regge-pole parametrization performed in Ref. 36.

In the region of small masses, we write the πN scattering amplitude in the center-of-mass system, using two-component spinors:

$$T(s,t) = T(s,z) = 8\pi\sqrt{s}\,\varphi_2^+ (f(s,z) + g(s,z)\,\boldsymbol{\sigma}\times\mathbf{n})\,\varphi_1; \qquad \text{(A.1)}$$

where z is the cosine of the scattering angle; $\mathbf{n}$ is the vector of the normal to the reaction plane.

The amplitudes f and g can be expressed in the standard manner in terms of the phase shifts and the inelasticity coefficients, which were tabulated for the calculations and taken from Ref. 35. It was assumed that f and g do not change as functions of the cosine of the scattering angle z when the amplitude leaves the mass shell, so that the entire dependence on the virtual mass is factorized and contained in the form factors F_2 or F_1. In Eq. (A.1) the scattering angle (for example, for the upper block in Fig. 6a) was taken to be the angle between the initial and the created proton in the center-of-mass system of the $p\pi^+$ pair. If the amplitude is expressed thus, the differential cross sections with respect to the cosine of this angle automatically coincide with the differential cross sections of the elastic amplitudes on the mass shell.[10)]

In the region of large masses, in order to express the amplitudes without changing the helicity of $\tilde{f}$ but changing $\tilde{g}$, Regge-pole parametrization with poles p, p', and ρ was used[36]:

$$\begin{aligned}\tilde{f}_i &= \gamma_{fi}\eta_i \exp\{(\alpha_i(0)-1)\ln E_L \\ &\quad + [R_i^2 + \alpha i' (\ln E_L - i(\pi/2))]\,t\}\,2Q; \\ \tilde{g}_i &= \tilde{f}_i \gamma_{gi}\sqrt{|t|}/2\gamma_{fi}, \quad i = p,\ p',\ \rho.\end{aligned} \qquad \text{(A.2)}$$

Here, Q is the modulus of the three-momentum in the center-of-mass system; E_L and t are the laboratory energy and the square of the momentum transfer (in GeV); γ_{fi} and γ_{gi} are the residues of the Regge poles at $t=0$; $\alpha_i(0)$ and α'_i are the parameters of the trajectories $\alpha_i(t) = \alpha_i(0) + \alpha'_i$; R_i^2 are the radii which characterize the dependence of the residues on t, these being assumed equal for the two amplitudes; η_i are the signature factors $\eta_p = i$, $\eta_{p'} = i-1$, $\eta_\rho = -i-1$.

The values of the free parameters and the parameters of the trajectories were taken from Ref. 36 and are given in Table A.1.

The amplitudes corresponding to concrete channels can be expressed as follows:

$$\left.\begin{aligned} T_{\pi^+p} &= T_p + T_{p'} + T_\rho; \quad T_{\pi^-p\to\pi^0n} = \sqrt{2}\,T_\rho; \\ T_{\pi^-p} &= T_p + T_{p'} - T_\rho; \quad T_{\pi^0p} = T_p + T_{p'}. \end{aligned}\right\} \qquad \text{(A.3)}$$

We define the normalization of the amplitudes in terms of the differential cross section with respect to the solid angle:

$$d\sigma/d\Omega = |f|^2 + |g|^2 \sin^2\theta = |\tilde{f}|^2 + |\tilde{g}|^2. \qquad \text{(A.4)}$$

Since the natural variable for the functions $\tilde{f}$ and $\tilde{g}$ is the square of the momentum transfer t and not the cosine of the scattering angle z, it was assumed that $\tilde{f}$ and $\tilde{g}$ as functions of t do not change on the departure from the mass shell. The entire dependence on the departure from the mass shell was contained in the form factor. And, as we have noted above, in order to describe the experimental data better it is necessary to introduce an additional dependence on the virtual mass, contained in Eq. (16), for the contribution of the vacuum pole to the block of virtual πN and $\pi\pi$ scattering. To avoid a discontinuity at the fitting point $\sqrt{s} = 2$ GeV, the contribution of the vacuum pole in the form (A.2) was continued into the resonance region to the threshold. If the amplitudes obtained by phase-shift analysis and the vacuum pole are denoted by T_{psa} and T_p, then the off-shell amplitude in the mass range $\sqrt{s} < 2$ GeV, excluding

[10)] The presence in the form factor of the perpendicular components of the momenta of the pions tends to peak the angular distributions, but this is not important for us.

TABLE A.2. Parameters of the Regge-pole parametrization of the $\pi\pi$ scattering amplitudes, GeV.

Parameter	$\alpha_i(0)$	$\alpha_i'(0)$	γ_i	R_i^2
p	1.0	0.5	1.4	1.4
p'	0.5	1.0	1.2	2.0
ρ	0.5	1.0	0.84	2.0

the dependence contained in the form factor, has the form [see also (16)]:

$$T(t)=T_{\text{psa}}(\mu^2)+T_p(\mu^2)\,[\exp\{R_p^2(t-\mu^2)\}-1].$$

In the calculations, the factor $2Q$ in (A.2) was replaced by $\sqrt{s}$ in the nonvacuum poles. In the region $s>9$ GeV^2 this change hardly affected the cross section, while at the point $\sqrt{s}=2$ GeV it was possible to obtain a better fit to the amplitudes obtained by phase-shift analysis. The greatest difference was obtained in the π^+p scattering channel, reaching about 30% there in the cross sections (see Figs. 10, 41, and 42). The poor fit is probably due to the shortcomings of the phase-shift analysis, which does not reproduce the cross section well in the region of the resonance $\Delta^{++}(1960)$.

2. Parametrization of $\pi\pi$ scattering amplitudes

The $\pi\pi$ scattering amplitudes were parametrized like the πN ones. In the region of small masses ($M_{\pi\pi}<1.4$ GeV), phase-shift analysis was used. The phase shifts and the inelasticity coefficients for the amplitudes with isospin $I\neq 2$ for $M_{\pi\pi}<1.1$ GeV were taken from Ref. 37, and in the region $1.1<M_{\pi\pi}<1.4$ GeV they were taken from Ref. 38. The amplitude with isospin $I=2$ was taken from Ref. 39.

In the region $M_{\pi\pi}>1.4$ GeV, Regge parametrization of the $\pi\pi$ scattering amplitude by means of the p, p', and ρ poles[12,13] was used in the form

$$T_i(s,t)=M_i(s,t)\,16\pi q_0\sqrt{s}=\eta_i(0)\,\gamma_i\,(s/s_0)^{\alpha_i(0)-1}\times\exp\{[R_i^2+\alpha_i'(\ln(s_1/s_0)-i\pi/2)]\,t\},\quad i=p,\ p',\ \rho,\qquad\text{(A.5)}$$

where $q_0=\sqrt{s-4\mu^2/2}$; $s_0=1$ GeV^2; $\eta_i(0)$ are the signature factors; $\alpha_i(0)$ and α_i' are the intercepts and slopes of the trajectories; $\gamma_i\exp(R_i^2t)$ are the residues; $\eta_i(0)=(1+\sigma_i\exp[-i\pi\alpha_i(0)])/\sin(\pi\alpha_i(0))$; $\sigma_p=\sigma_{p'}=1$, $\sigma_\rho=-1$.

Obviously, in the region $M_{\pi\pi}\sim 1.4$–2 GeV, in which resonances have frequently been observed [the most pronounced in the elastic channel is $G(1700)$], one cannot hope for more than an averaged description of the amplitude by means of smooth Regge terms. The values of the parameters γ_i and R_i^2 were chosen, first, to ensure the best fit of the Regge parametrization of the amplitudes of the different $\pi\pi$ channels at the point $M_{\pi\pi}=1.4$ GeV to the phase-shift analysis and, second, to describe the existing experimental distributions in the different reaction channels $\pi N\to\pi\pi N$ in the region of masses $M_{\pi\pi}>1.4$ GeV.

The different $\pi\pi$ scattering channels were parametrized as follows:

$$\left.\begin{aligned}
\langle\pi^+\pi^+\,|\,T\,|\,\pi^+\pi^+\rangle&=\tilde{M}_{\tilde{p}}(s,t)+M_\rho(s,t)+\tilde{M}_{\tilde{p}}(s,u)+M_\rho(s,u);\\
\langle\pi^+\pi^-\,|\,T\,|\,\pi^+\pi^-\rangle&=\tilde{M}_{\tilde{p}}(s,t)-M_\rho(s,t);\\
\langle\pi^\pm\pi^0\,|\,T\,|\,\pi^\pm\pi^0\rangle&=\tilde{M}_{\tilde{p}}(s,t)+M_\rho(s,u);\\
\langle\pi^0\pi^0\,|\,T\,|\,\pi^+\pi^-\rangle&=M_\rho(s,t)+M_\rho(s,u);\\
\langle\pi^0\pi^0\,|\,T\,|\,\pi^0\pi^0\rangle&=\tilde{M}_{\tilde{p}}(s,t)+\tilde{M}_{\tilde{p}}(s,u).
\end{aligned}\right\}\qquad\text{(A.6)}$$

Here, $\tilde{M}_p=M_p+M_{p'}$. In these equations, allowance is made for the exchange of reggeons in not only the t but also the u channel.

At the point $M_{\pi\pi}=1.4$ GeV the total cross section σ_{tot}, the elastic cross section σ_{el}, the differential cross section at 0°, namely, $d\sigma/d\Omega(0°)$, and the effective slope with respect to the momentum transfer were fitted (for each channel). For the fitting, the parameters $\alpha_i(0)$ and α_i' were fixed, and the parameters γ_i and R_i^2 varied. The values of all the parameters are given in Table A.2.

[1]K.A. Ter-Martirosyan, Zh. Éksp. Teor. Fiz. 44, 341 (1963) [Sov. Phys. JETP 17, 233 (1963)].
[2]H.M. Chan, J. Loskiewicz, and W.W.M. Allison, Preprint TH CERN (1968).
[3]G. Wolf, Phys. Rev. 182, 1538 (1969).
[4]E.L. Berger, Phys. Rev. Lett. 21, 701 (1968).
[5]J.W. Dash, J. Huskins, and S.T. Jones, Preprint ANL/HEP 7355 (1973); J.W. Dash and S.T. Jones, Preprint ANL/HEP 7371 (1974).
[6]F.T. Dao *et al.*, Phys. Rev. Lett. 30, 34 (1973).
[7]P. Chliapnikov *et al.*, Preprint CERN/D. Ph. 11/Phys. 71-44 (1971).
[8]G. Grayer *et al.*, Phys. Lett. B 39, 563 (1972).
[9]C. Michael, Preprint TH 1567-CERN (1972).
[10]K.G. Boreskov *et al.*, Yad. Fiz. 15, 361 (1972) [Sov. J. Nucl. Phys. 15, 203 (1972)].
[11]K.G. Boreskov *et al.*, Yad. Fiz. 15, 557 (1972) [Sov. J. Nucl. Phys. 15, 309 (1972)].
[12]K.G. Boreskov, A.B. Kaĭdalov, and L.A. Ponomarev, Yad. Fiz. 17, 1285 (1973) [Sov. J. Nucl. Phys. 17, 669 (1973)].
[13]K.G. Boreskov, A.B. Kaĭdalov, and L.A. Ponomarev, in: Lektsii na Shkole Fiziki Élementarnykh Chastits (Lectures at the School of Elementary-Particle Physics), Erevan, 1971; Preprint ITÉF No. 50 /in Russian/ (1972).
[14]K.G. Boreskov, A.B. Kaĭdalov, and L.A. Ponomarev, in: Lektsii na Pervoi Shkole Fiziki ITÉF (Lectures at the First School of Physics of the Institute of Theoretical and Experimental Physics), Atomizdat, Moscow (1973).
[15]K.G. Boreskov, A.B. Kaĭdalov, and L.A. Ponomarev, Preprint ITÉF-16 /in Russian/ (1974).
[16]K.G. Boreskov *et al.*, Preprint JINR R1-8163 /in Russian/, Dubna (1974).
[17]K.G. Boreskov *et al.*, Preprint JINR R1-8164 /in Russian/, Dubna (1974).
[18]E. Colton *et al.*, Phys. Rev. D 3, 1063 (1971).
[19]P. Kobe, H.J. Mück, and U. Idschok, Nucl. Phys. B 52, 109 (1973).
[20]M. Derrick *et al.*, Preprint ANL/HEP 7354 (1974).
[21]K. Gottfried and J.D. Jackson, Nuovo Cimento 33, 309 (1964).
[22]A.B. Kaĭdalov and B.M. Karnakov, Yad Fiz. 7, 152 (1968) [Sov. J. Nucl. Phys. 7, 111 (1968)].
[23]L. Stodolsky and J.J. Sakurai, Phys. Rev. Lett. 11, 90 (1963).
[24]M. Boratav, J. Le Guyader, and M. Sene, Nucl. Phys. B 20, 573 (1970).
[25]G.V. Beketov *et al.*, Preprint ITÉF-68 /in Russian/ (1973).
[26]V.V. Glagolev *et al.*, Preprint JINR R1-6846 /in Russian/, Dubna (1972).
[27]R. Honecker *et al.*, Nucl. Phys. B 50, 157 (1972).
[28]G.V. Beketov *et al.*, Yad. Fiz. 20, 717 (1974) [Sov. J. Nucl. Phys. 20, 384 (1975)].

[29]M.J. Losty, Preprint CERN I D. Ph. 11/Phys., 73-26 (1973).
[30]A.N. Didens, Rapporteur's Talk at XVII International Conference on High Energy Physics, London (1974).
[31]E. Colton *et al.*, Phys. Rev. D **7**, 3267 (1973).
[32]P. Kobe, H.J. Mück, and U. Idschok *et al.*, Nucl. Phys. B **52**, 109 (1973).
[33]S. Pokorsky and H. Satz, Preprint TH-1088 CERN, 19769.
[34]U. Amaldi, Rapporteur's Talk at VII Conference on Elementary Particles, Aix-en-Provence (1973).
[35]P. Bareyre, C. Brieman, and C. Villet, Phys. Rev. **165**, 1730 (1968).
[36]V. Yu. Glebov *et al.*, Yad. Fiz. **10**, 1065 (1969) [Sov. J. Nucl. Phys. **10**, 609 (1970)].
[37]S.D. Protopopescu *et al.*, Phys. Rev. D **7**, 1279 (1973).
[38]D. Cohen, Phys. Rev. D **7**, 661 (1973).
[39]J.T. Carroll *et al.*, Phys. Rev. Lett. **28**, 318 (1970).
[40]Z. Ming Ma *et al.*, Phys. Rev. Lett. **23**, 342 (1969).
[41]S.P. Almeida *et al.*, Phys. Rev. **174**, 1638 (1969).
[42]H. Bøggild *et al.*, Proc. of the XV Conf. on High Energy Phys., Kiev (1970).
[43]L. Lyons, Nucl. Phys. B **15**, 355 (1970).

Translated by Julian B. Barbour